



OPEN ACCESS

EDITED BY

Paraskevi Polymenakou,
Hellenic Centre for Marine Research
(HCMR), Greece

REVIEWED BY

Carmen Rizzo,
Anton Dohrn Zoological Station
Naples, Italy
Mary Thaler,
Laval University, Canada

*CORRESPONDENCE

Anabel von Jackowski
✉ anabel.vonjackowski@obs-banyuls.fr
Massimiliano Molari
✉ mamolari@mpi-bremen.de

†PRESENT ADDRESS

Anabel von Jackowski,
CNRS/Sorbonne Université, UMR7621
Laboratoire d'Océanographie Microbienne,
Banyuls-sur-Mer, France

RECEIVED 03 May 2023

ACCEPTED 29 September 2023

PUBLISHED 31 October 2023

CITATION

von Jackowski A, Walter M, Spiegel T,
Buttigieg PL and Molari M (2023) Drivers of
pelagic and benthic microbial communities
on Central Arctic seamounts.
Front. Mar. Sci. 10:1216442.
doi: 10.3389/fmars.2023.1216442

COPYRIGHT

© 2023 von Jackowski, Walter, Spiegel,
Buttigieg and Molari. This is an open-access
article distributed under the terms of the
[Creative Commons Attribution License
\(CC BY\)](https://creativecommons.org/licenses/by/4.0/). The use, distribution or
reproduction in other forums is permitted,
provided the original author(s) and the
copyright owner(s) are credited and that
the original publication in this journal is
cited, in accordance with accepted
academic practice. No use, distribution or
reproduction is permitted which does not
comply with these terms.

Drivers of pelagic and benthic microbial communities on Central Arctic seamounts

Anabel von Jackowski^{1*†}, Maren Walter², Timo Spiegel³,
Pier Luigi Buttigieg⁴ and Massimiliano Molari^{1*}

¹HGF-MPG Group for Deep Sea Ecology and Technology, Max Planck Institute for Marine Microbiology, Bremen, Germany, ²Marine Geochemistry, MARUM – Center for Marine Environmental Sciences, University of Bremen, Bremen, Germany, ³HGF-MPG Group for Deep Sea Ecology and Technology, GEOMAR Helmholtz Centre for Ocean Research Kiel, Kiel, Germany, ⁴Alfred Wegener Institute, Helmholtz Centre for Polar and Marine Research, Bremerhaven, Germany

Seamounts are abundant features on the seafloor that serve as hotspots and barriers for the dispersal of benthic organisms. The primary focus of seamount ecology has typically been on the composition and distribution of faunal communities, with far less attention given to microbial communities. Here, we investigated the microbial communities in the water column (0–3400 m depth) and sediments (619–3883 m depth, 0–16 cm below seafloor) along the ice-covered Arctic ridge system called the Langseth Ridge. We contextualized the microbial community composition with data on the benthic trophic state (i.e., organic matter, chlorophyll-*a* content, and porewater geochemistry) and substrate type (i.e., sponge mats, sediments, basaltic pebbles). Our results showed slow current velocities throughout the water column, a shift in the pelagic microbial community from a dominance of Bacteroidia in the 0–10 m depth towards Proteobacteria and Nitrososphaeria below the epipelagic zone. In general, the pelagic microbial communities showed a high degree of similarity between the Langseth Ridge seamounts to a northern reference site. The only notable differences were decreases in richness between ~600 m and the bottom waters (~10 m above the seafloor) that suggest a pelagic-benthic coupling mediated by filter feeding of sponges living on the seamount summits. On the seafloor, the sponge spicule mats, and polychaete worms were the principal source of variation in sedimentary biogeochemistry and the benthic microbial community structure. The porewater signature suggested that low organic matter degradation rates are accompanied by a microbial community typical of deep-sea oligotrophic environments, such as Proteobacteria, Acidimicrobiia, Dehalococcoidia, Nitrospira, and archaeal Nitrososphaeria. The combined analysis of biogeochemical parameters and the microbial community suggests that the sponges play a significant role for pelagic-benthic coupling and acted as ecosystem engineers on the seafloor of ice-covered seamounts in the oligotrophic central Arctic Ocean.

KEYWORDS

Arctic, seamount, water column, sediments, porewater, microbes

1 Introduction

Seamounts are abundant topographical features that rise at least 100 m to many 1000 m above the seafloor as isolated or clustered underwater mountains (Yesson et al., 2011). There are an estimated 100,000 to over 25 million seamounts in the ocean (Kitchingman and Lai, 2004; Wessel et al., 2010). As obstacles to ocean currents, seamounts can modify the physical oceanographic conditions, including vertical mixing, internal waves, the local current system in the form of Taylor caps, and trapping mesoscale ocean eddies (Royer, 1978; Roden, 1987; Roden, 1991; Chapman and Haidvogel, 1992; Beckmann and Mohn, 2002; Lavelle and Mohn, 2010).

Several decades of observational research have shown that seamounts are “hotspots” of marine life. The physical oceanography at seamounts can enhance biomass, species diversity, and production in the water column, which is referred to as the “seamount effect” (Dower and Mackas, 1996). For example, the Cobb Seamount enhances the phytoplankton composition but not its biomass (Dower and Mackas, 1996), at Great Meteor Seamount repeated surveys showed a high degree of temporal and spatial variability in phytoplankton response (Mouriño et al., 2001), and Senghor Seamount revealed a substantial effect of several-fold particulate matter export suggesting a possible phytoplankton response (Turnewitsch et al., 2016). Each seamount presents a unique case study with some that show a response by pelagic microbial communities (here, bacteria and archaea), while other seamounts do not (Mendonça et al., 2012; Djurhuus et al., 2017a; Djurhuus et al., 2017b; Zhao et al., 2022). The role of seamounts in ocean productivity is still in its infancy, but seamount summits as habitats for sessile epifauna like deep water corals, sea anemones, and sponges has been well-documented (Genin et al., 1986; Consalvey et al., 2010; Miller and Gunasekera, 2017; Morganti et al., 2022). The volcanic origin of many seamounts creates a steep topography, allowing a high proportion of hard substrata to settle compared to other deep-sea ecosystems (Rogers, 2018). If seamounts remain hydrothermally active, the chemical exchange between crust and ocean (Villinger et al., 2002; Harris et al., 2004; Fisher, 2010; Villinger et al., 2017) and hydrothermal fluids support chemosynthesis-based food webs with vent fauna (e.g., tube worms) and hydrothermal-vent-associated microbes (e.g., Epsilonproteobacteria) (Emerson and Moyer, 2010). At inactive hydrothermal seamounts, hydrothermal circulation can be driven by the cooling of the lithosphere with oxygenated and nitrogen-rich seawater (Fisher, 2010; Klügel et al., 2020). In particular, systematic analyses and multidisciplinary studies on biogeochemical parameters and microbes at inactive seamounts are still lacking, although seamounts offer an ideal study system with steep environmental gradients across narrow spatial scales.

The Gakkel Ridge in the Arctic Ocean has very few, small volcanic seamounts in the west and seamount clusters near the large magmatic centers in the east (Cochran, 2008). Small volcanic seamounts are a dominant morphologic feature of slow-spreading mid-ocean ridges, ranging between 6.5 mm yr⁻¹ to 12.8 mm yr⁻¹

along the Gakkel Ridge (Karasik, 1968; Taylor et al., 1979; DeMets et al., 1994; Brozena et al., 2003; Cochran, 2008). Bathymetric surveys separated the Gakkel Ridge into three sections: the Western Volcanic Zone extends from 7°W to 3°E, the Sparsely Magmatic Zone extends from 3°E to 29°E, and the Eastern Volcanic Zone extends from about 29°E eastwards. In particular, the Eastern Volcanic Zone suggests recent volcanism and two distinct changes in the ridge axis in the form of perpendicular bathymetric ridges at 30°E and 62°E that are possibly tectonic rather than volcanic origin. (Cochran et al., 2003; Michael et al., 2003). The aim of this study was to characterize the seamount cluster at the 62°E axial ridge with three individual peaks, called the Langseth Ridge. We investigated current dynamics, benthic biogeochemistry, the pelagic and benthic microbial diversity (based on 16S rRNA gene sequencing). The study explores the effect of the seamount on local seawater stratification and whether the trophic status or the substrate are the major drivers in shaping benthic microbial communities. We hypothesized that differences in organic matter deposition influence the Langseth Ridge microbial communities but also that organic matter deposition varies substantially with substrate nature across the heterogeneous surface of the seamount (Morganti et al., 2021; Morganti et al., 2022).

2 Materials and methods

2.1 Study area

Water column and benthic samples were collected between 16th September and 9th October 2016 as part of the *RV Polarstern* expedition PS101. The sampling focused on the Langseth Ridge, which extends over 60 km in length and 600 m to 4860 m below sea level. Specifically, eight locations along Langseth Ridge were sampled: Northern Seamount, Central Seamount, Seamount Saddle (sediment only), Karasik Seamount, Southern Slope (sediment only), Polaris Vent (sediment only), “N-Reference”, and “S-Reference” (Figure 1; Tables 1, 2, S1). The seamount summits were partially covered by large sponges and their silica needles that formed mats on the seafloor, biological remnants from worm tubes and shells, further referred to as “biological debris”, and some sedimented material (Morganti et al., 2022).

2.2 Sample collection

In situ current data was recorded during PS101 using a TRDI 300 kHz Workhorse Monitor as a Lowered acoustic Doppler current profiler (LADCP) system (Boetius and Purser, 2017). The LADCP was mounted to the CTD/rosette where the abundance of scatters in the water column was sufficient to return good quality acoustic data. The raw data were post-processed using an inverse method (Visbeck, 2002), resulting in an accuracy of ± 0.03 m s⁻¹. Additionally, long-term current information was retrieved from a mooring near the N-

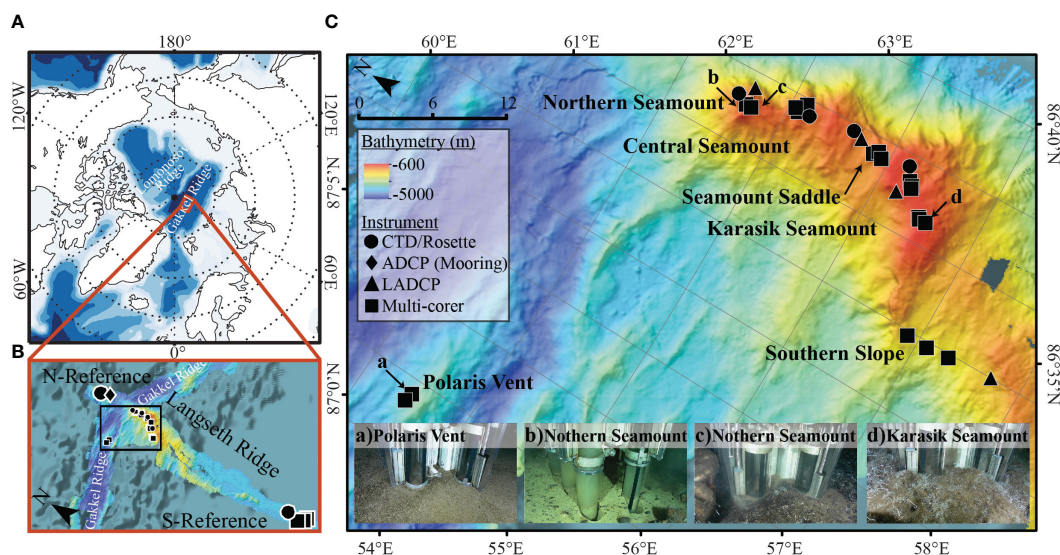


FIGURE 1 Bathymetric maps showing the Arctic Ocean with the Gakkel Ridge and the perpendicular Langseth Ridge. The (A) regional bathymetric map shows the location of the Langseth ridge with respect to the major landmasses in the Arctic. The Gakkel Ridge is intersected by a perpendicular bathymetric ridge, called the (B) Langseth Ridge, characterized by (C) three seamounts. We sampled the three seamounts, the Seamount Saddle, and the Southern Slope, with the nearby Polaris Vent, N-Reference (water), and S-Reference (sediment) using a Conductivity, Temperature, and Depth (CTD) sampler (circle), stationary acoustic Doppler current profilers (ADCP; diamond) and lowered ADCP (LADCP; triangle), and multi-corer (MUC; square). Images in (C) show the heterogeneity of the sediment cores along the Langseth Ridge from (a) Polaris Vent PS101/187-1, (b, c) Northern Seamount PS101/195-1 and PS101/196-1, and (d) Karasik Seamount PS101/104-1.

Reference (PS101/113-1, Table 1). The mooring was equipped with three current meters: two ADCPs (one upward-looking, one downward-looking) and one single point recording current meter (RCM7, Aanderaa) (von Appen et al., 2017).

Discrete water samples were collected at four locations using a CTD/rosette (SBE911plus, Sea-Bird Electronics, Inc.). The CTD was equipped with two temperature probes, two conductivity

probes, a Digiquartz pressure sensor, an oxygen sensor (SBE 43), a fluorometer (WET Labs ECO-AFL/FL), a transmissometer (WET Labs C-Star), and an altimeter, attached to a rosette carousel with 12-L Niskin bottles (Boetius and Purser, 2017). Water column samples were acquired at the surface (0-50 m), 200 m, 400 m, 600 m, and 10 m above the seafloor at each site (here “bottom water”, Table 1). After CTD/rosette recovery, 8-10 L of seawater was filtered

TABLE 1 Water column samples were acquired along Langseth Ridge locations during the RV *Polarstern* (PS101) in the fall of 2016 (Boetius and Purser, 2017).

Location	Device	Station	Latitude N (DD)	Longitude E (DD)	Sampling Depths (m)
Northern-Reference	CTD	PS101/175-1	87.10	61.61	1.4, 50.2, 200.0, 1000.0, 2000.0, 2998.7, 3342.4
	ADCP-1	PS101/113-1	87.02	59.26	0-220
	ADCP-2	PS101/113-1	87.02	59.26	270-420
	RCM	PS101/113-1	87.02	59.26	773
Southern-Reference	CTD	PS101/055-1	85.29	60.16	no DNA samples collected
Northern Seamount	CTD	PS101/172-1	86.87	61.59	1.3, 200.3, 391.2, 604.1, 618.7
	LADCP	PS101/202-1	86.86	61.48	0-730
Central Seamount	CTD	PS101/097-1	86.82	61.73	51.4, 200.0, 400.3, 600.4, 853.1
	CTD	PS101/149-1	86.80	61.84	1.7, 202.2, 401.2, 600.0, 750.7
Seamount Saddle	LADCP	PS101/213-1	86.77	61.84	0-550
Karasik Seamount	CTD	PS101/126-1	86.74	61.86	12.3, 200.4, 394.3, 600.6, 715.5
	LADCP	PS101/192	86.74	61.45	0-510
Southern Slope	LADCP	PS101/224	86.61	59.96	0-1610

The max sampling depth was 10 m above the seafloor. Conductivity, Temperature, and Depth sampler, CTD; Acoustic Doppler Current Profiler, ADCP; Lowered Acoustic Doppler Current Profiler, LADCP; Recording Current Meter, RCM.

TABLE 2 Sediment samples along Langseth Ridge locations during the RV *Polarstern* (PS101) in the fall of 2016 (Boetius and Purser, 2017).

Location	Device	Station	Latitude N (DD)	Longitude E (DD)	MUC Sampling Depth (m)	MUC Core length (cm)
Southern-Reference	MUC	PS101/061-1	85.24	59.96	3883	16 *
	MUC	PS101/062-1	85.23	60.01	3880	16 *
	MUC	PS101/063-1	85.21	60.01	3880	22
Northern Seamount	TV-MUC	PS101/195-1A	86.86	61.58	639	14 *
	TV-MUC	PS101/195-1B	86.86	61.58	639	16 *
	TV-MUC	PS101/196-1	86.86	61.62	657	16 *
Central Seamount	TV-MUC	PS101/151-1	86.83	61.77	860	8
	TV-MUC	PS101/152-1	86.83	61.65	903	6 *
	TV-MUC	PS101/205-1	86.83	62.01	1183	16 *
Seamount Saddle	TV-MUC	PS101/210-1	86.76	61.74	888	6 *
	TV-MUC	PS101/211-1	86.76	61.81	909	16
	TV-MUC	PS101/212-1	86.77	61.77	957	6 *
Karasik Seamount	TV-MUC	PS101/123-1	86.74	61.63	651	7
	TV-MUC	PS101/125-1A	86.73	61.61	656	6 *
	TV-MUC	PS101/125-1B	86.73	61.61	656	6 *
	TV-MUC	PS101/101-1	86.71	61.61	635	11
	TV-MUC	PS101/102-1	86.71	61.30	643	6 *
	TV-MUC	PS101/104-1	86.71	61.32	637	16 *
Southern Slope	TV-MUC	PS101/218-1	86.68	59.94	1852	23
	TV-MUC	PS101/219-1	86.66	59.92	2049	16 *
	TV-MUC	PS101/220-1	86.64	59.95	2002	16 *
Polaris Vent	TV-MUC	PS101/140-1A	86.96	55.79	3263	13
	TV-MUC	PS101/140-1B	86.96	55.79	3263	16 *
		PS101/187-1	86.96	55.78	3410	25

The multi-corer (MUC) was used to sample the sediment, with an additional glass fiber cable (TV-MUC) that supplied images at most stations. (*) Samples were not processed for porewater analysis.

through 0.22-µm pore-sized STERIVEX filters (Merck-Millipore, USA) using a peristaltic pump and stored frozen at -40°C until further processing.

Discrete sediment samples were collected using a multi-corer (MUC) from all eight locations (Table 2). The MUC was deployed three times at each location that served as biological replicates and most deployments were camera-guided (TV-MUC), which allowed for local seafloor imaging (Figure 1; Table S2). In total, 24 undisturbed sediment cores were retrieved for biogeochemical and genetic analysis (Boetius and Purser, 2017). After the MUC recovery, the cores were transferred into a temperature-controlled laboratory (+2°C) for further processing. If present, biological debris above the sediment (i.e., sponge and/or polychaete worm debris) was removed prior to pore water sampling and sediment slicing (Table S2). Then, porewater extractions were performed on one core from each location, with the exception of two cores at the Polaris Vent (PS101/140-1A and PS101/187-1) and Karasik Seamount (PS101/101-1 and PS101/123-1), using Rhizons extractions in 1 cm intervals (SMS type MOM, 19.21.21F; mean pore size: 0.15 µm; Rhizosphere Research Products; Böer et al., 2009) and were stored (+4°C) until analysis. Finally, cores were sliced into sections (0-1 cm, 1-2 cm, 2-3 cm, 3-5 cm, and 14-16 cm), stored in 50 mL falcons, and frozen (-20°C) until further analysis.

2.3 Sample and data analysis

2.3.1 DNA extraction, sequencing, and pipeline

DNA was extracted from the water filters and sliced sediment. For the water samples, 27 STERIVEX filters were extracted using the PowerWater® DNA Isolation Kit (Qiagen, Germany). For the sediment, 62 samples from 0-1 cm, 3-5 cm, and 14-16 cm were extracted using the MoBio FastDNA™ Spin kit (MP Biomedicals, USA). 0.5 g of homogenized sediment was used for the kit, according to the manufacturer’s instructions. The concentration and purity (absorption ratio: 260 nm/280 nm; inclusion threshold >2) of the extracts was measured using the infinite200™ Nanoquant (Tecan, Crailsheim, Germany).

Illumina Miseq library preparation and paired-end tag sequencing (2 x 300 bp) were performed in triplicate at the Center for Biotechnology, University of Bielefeld, Bielefeld, Germany according to the standard instructions of the 16S Metagenomic Sequencing Library Preparation protocol (Illumina, Inc., USA). In addition to the samples, ultrapure Milli-Q water (Thermo Fisher Scientific, USA; Product 10977049) was amplified and sequenced to serve as a negative control and identify sequencing contaminants. The 16S rRNA genes were amplified using three primers: water column bacteria and archaea using v4v5 region with primers 515F (GTGYCAGCMGCCGCGGTAA) and 926R

(CCGYCAATTYMTTTRAGTTT) (Parada et al., 2016), sediment-bacteria using v3v4 region using primers S-D-Bact-0341-b-S-17 (CCTACGGGNGGCWGCAG) and S-D-Bact-0785-a-A-21 (GACTACHVGGGTATCTAATCC) (Klindworth et al., 2013), and the sediment-archaea using v3v5 region with Arch349F (GTGYCAGCMGCCGCGGTAA) and Arch915R (CCGYCAATTYMTTTRAGTTT) (Amann et al., 1990; Klindworth et al., 2013) (Figure S1).

Illumina raw reads were processed using a modification of the pipeline of Hassenrück et al. (2016). The full pipeline and scripts are available at <https://github.com/anelvonjackowski/Publications>. In brief, sequence adaptors and primers were clipped using cutadapt (Martin, 2011), allowing a mismatch proportion error of 0.16. The water column and sediment-bacteria FASTQ files were trimmed using trimmomatic (v0.35; Bolger et al., 2014) with a sliding window of 4 and quality threshold of 10 (4:12 for v3v5) and a minimum read length of 100 base pairs. Thereafter, paired-end reads were merged using PEAR (v0.9.6; Zhang et al., 2014) with a minimum overlap of 10 and a minimum length of 350. The sediment-archaea FASTQ files were first merged and thereafter clipped. Finally, reads were clustered using swarm (v2.2.2; Mahé et al., 2014) and classified against the SILVA SSU Reference dataset (release 132, 2018) reference database using the SINA aligner (v1.2.11; Pruesse et al., 2012). Operational Taxonomic Units (OTUs) matching chloroplast and mitochondrial sequences were excluded from further analyses. The sequences were deposited at the European Nucleotide Archive (ENA) under accession number PRJEB34976, with data submission brokered by the German Federation for Biological Data (GFBio; Diepenbroek et al., 2014).

Data were imported, stored, and analyzed using the phyloseq package (v1.42.0; McMurdie and Holmes, 2013) and ggplot2 package (v3.4.2; Wickham, 2016) with aesthetic modifications of figures using Adobe Illustrator. Absolute singletons, OTUs with a single sequence in the whole data set, were removed prior to statistical analysis. Negative controls were removed from the datasets, except for the v4v5 primer since negative controls were not available (Supplementary Methods). For each sample in our OTU matrix, we calculated the richness, estimated richness (chao1), Shannon-Wiener, and Inverse Simpson diversity indices. Chao1 indices were calculated with 999 random re-sampling runs to account for differences in sequencing depth between samples. Non-metric multidimensional scaling (NMDS) was applied using phyloseq in combination with compositions package (v2.0.6, function “clr” method central-log transformed) based on euclidean distances. An ANalysis Of SIMilarity (ANOSIM) was performed on the clr transformed dissimilarity matrix and euclidean distances (phyloseq package function “phyloseq::distance”) using vegan package (v2.6-4; function “anosim”).

The fold-change (FC) in the water column and sediment was analyzed following the script by Fadeev (2018). The abundance of each OTU was calculated using the DESeq2 package (v1.38.3), followed by a taxonomic enrichment test using GAGE package (v2.48.0), and corrected for multiple testing (Benjamini and Hochberg, 1995). For the water column, FC was tested on depth based on the four NMDS clusters: 0-10 versus 50 m, 50 m versus 200 m-400 m-600 m-bottom waters (seamount), and bathypelagic depths (only N-Reference). In the sediment, FC was tested on the location and layer depth based on NMDS clusters: surface and subsurface sediment layers at the

seamount versus Polaris Vent and S-Reference, and deep sediment layers at the seamount versus Polaris Vent and S-Reference. The FC was reported for differential abundances at the class and genus level absolute values higher than 1 or -1 and an adjusted p-value < 0.05.

2.3.2 Sediment biogeochemistry

The extracted porewater was analyzed for inorganic nutrients, dissolved inorganic carbon (DIC), total alkalinity (TA), sulfate, and sulfide. Inorganic nutrients (NO_2^- , NO_3^- , PO_4^{3-} , SiO_4 , NH_4^+) were measured using a Continuous Flow Nutrient Analyzer (QuAAtro 39, Seal Analytical) (Hansen and Koroleff 2007). DIC was measured using a flow injection system equipped with a Spark Optimas Auto-Sampler Model 820 (Böer et al., 2009). TA was measured using the Metrohm 794 Basic Titrino pH electrode (Dickson, 1981). Sulfate (SO_4^{2-}) and sulfide (S^{2-}) reacted with the 2% zinc-acetate solution and were quantified in a spectrophotometer (Cline, 1969).

The sliced sediment samples were analyzed for chloroplastic pigment equivalents (CPE) and organic matter concentration. CPE was extracted using acetone and measured as fluorescence (Trilogy, Turner Designs, USA) (Lorenzen, 1967), which allowed differentiation between chlorophyll-*a* (chl-*a*) and phaeopigments. Chl-*a* contribution was calculated from the ratio of chl-*a*-to-CPE. The total organic carbon (TOC) and total organic nitrogen (TON) were measured using an elemental analyzer (Flash EA 1112 coupled to Mas 200, Thermo Scientific, USA) (Kirsten, 1979).

2.3.3 Interpreting environmental conditions on community composition

All statistical tests were conducted in Rstudio running R (v4.2.1). Mann-Whitney tests were performed to test for significant differences for multiple profiles from the same location, e.g., two porewater cores at Polaris Vent (PS101/140-1A and PS101/187-1). Principal components analysis (PCA) was performed using FactoMineR package (v2.8) for porewater and sedimentary data to explore the relationships between “location”, “layer”, and “substrate”. Analysis of variance (ANOVA) and permutational multivariate ANOVA (PERMANOVA) using vegan package (function “adonis2”) tested the effect of “location”, “layer”, and “substrate” on environmental conditions within standardized (function “decostand”) porewater data and sedimentary data. A mixed-effects model with “sediments core” as a random factor and ANOVA were applied to test the significance of the “location”, “layer”, and “substrate” with lambda transformed to achieve a normal distribution for each sedimentary variable using nlme package (v3.1-162, function “lme”). Multifactorial ANOVA (MANOVA) was performed on “location”, “layer”, and “substrate” with the layer nested in the substrate. The interacting design was chosen to consider the presence of biological debris on top of sediments at some stations of Langseth Ridge, which depending on the thinness of the debris deposit, may prevent/reduce the exposure of sediments to the bottom water. Redundancy analysis (RDA) and ANOVA were performed to investigate to what degree sedimentary variables may explain variance in bacterial and archaeal community structure. In preparation for the RDA analysis, variables were assessed for collinearity using variance inflation factors (VIF) in usdm package (v.1.1-18, function “vif”). Variables with VIF<4 were retained, namely: CPE, chl-*a* contribution, TOC, and C:N ratio. The

RDA was performed in vegan package (function “rda”) for all layers (0-1 cm, 3-5 cm, and 14-16 cm) and repeated independently for the surface layer (0-1 cm).

3 Results

3.1 Water column

3.1.1 Oceanography

The water column was highly stratified with cold water at the surface, transformed Atlantic water (TAW) between 200-600 m, and deep-water masses below 600 m (Figures 2, S2; Tables 1, S1). Stratification was driven by salinity that formed polar halocline waters with gradually increasing salinities below the surface to 200 m depth. In this depth range, the mean temperature was $-0.76 \pm 1.03^\circ\text{C}$ and had a mean salinity of 33.86 ± 1.20 . Between 200 and 400 m depth, relatively warm water with a mean temperature of $1.25 \pm 0.19^\circ\text{C}$ and high salinity of 34.86 ± 0.03 are indicative of a TAW layer ($>-1.5^\circ\text{C}$ and $\sim 34.97 \text{ g kg}^{-1}$). Below the TAW, a temperature mean of $-0.08 \pm 0.56^\circ\text{C}$ and salinity of 34.90 ± 0.02 suggest mixing with the Arctic deep water below and gradually transforming into an Arctic deep water mass.

The local currents at the time of the observations were not influenced by the presence of the Langseth Ridge. The velocities are highest close to the surface (Figure 2), decreasing with depth, and generally lower than in the ridge valley to the north (not shown). For context, we also show the September monthly average of the mooring (PS101/113, close to N-Reference), positioned slightly northwest of the study area ($87^\circ 0.97' \text{N}$, $59^\circ 15.52' \text{E}$). During September 2016, the time of the synoptic observations, the

recorded average was $0.04 \pm 0.02 \text{ m s}^{-1}$ in a net westward direction, which indicates that the profile at the Northern Seamount (PS101/202) is fairly representative of the conditions north of the Langseth Ridge during the time of observations.

On the other side of the Gakkel Ridge rift valley, the surface currents increased from the north to the south. The ADCP profile velocities were highest at Seamount Saddle (PS101/213), exceeding 0.2 m s^{-1} at 30 m in a northwesterly direction (Figure 2). Within the TAW between 200 and 400 m, current speeds weakened to below 0.1 m s^{-1} at all stations. The flow in the TAW layer was generally westward (not shown), indicating a recirculation branch of the Atlantic Water (Schulz et al., 2021), and therefore “older” water that had been advected east in the boundary current closer to the continental slope along the Siberian shelf, and then detached at the Laptev Sea and returned west topographically steered by the Gakkel Ridge (Smith et al., 2021). Closer to the seafloor, the observed current speed increased at the Northern Seamount, while current speeds decreased at the Southern Slope (Figure 2).

3.1.2 Pelagic microbial community

The microbial community of the water column was targeted by the universal primer set (v4v5). The observed richness increased with water depth showing the highest richness in the 600 m samples, while evenness was highest in the 600 m and bottom water samples (Figures S3, S4). The non-metric multidimensional scaling (NMDS) ordination plot, based on euclidean distances and central-log transformed data, with 60% dissimilarity clusters indicated that communities clustered by water depth (ANOSIM $R=0.69$ $p=0.001$) but not by location (ANOSIM $R=0.04$, $p=0.24$; Figure 3A).

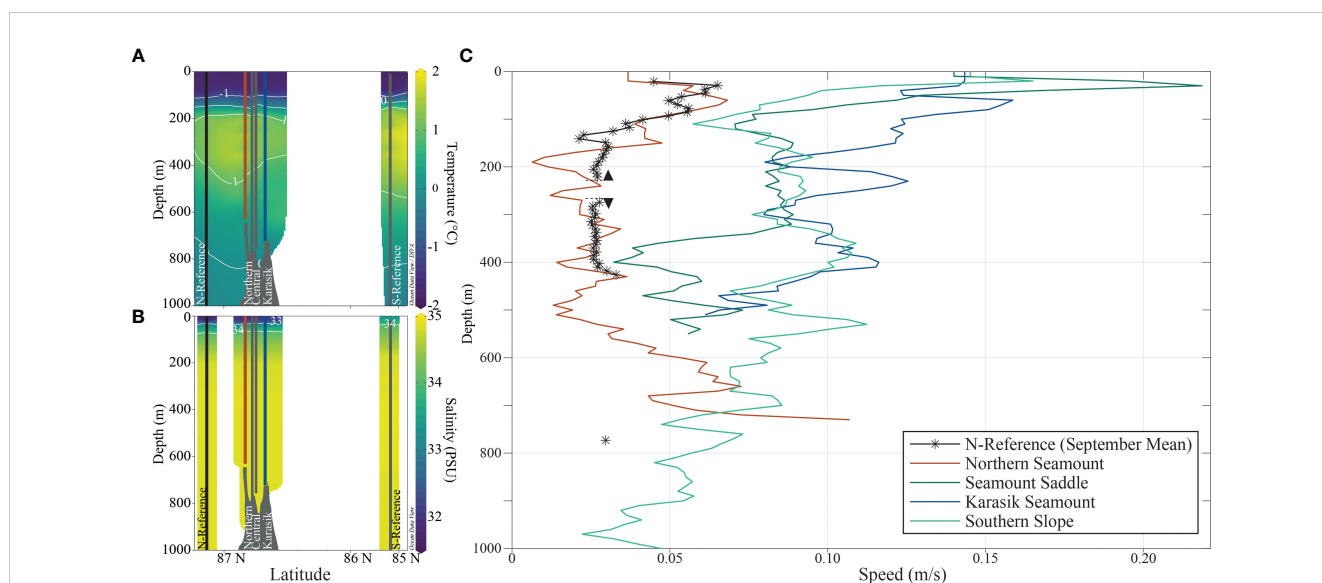


FIGURE 2 Oceanography in the upper 1000 m of the Langseth Ridge. The (A) temperature and (B) salinity were measured during the Conductivity, Temperature, and Depth (CTD) sampler casts at the Northern Seamount, Central Seamount, Karasik Seamount, N-Reference, and S-Reference. The (C) currents were measured using two stationary acoustic Doppler current profilers with one single point recording current meter at the N-Reference mooring (*) and lowered ADCPs (LADCP) at the Northern Seamount, Seamount Saddle, Karasik Seamount, and the Southern Slope. The arrowheads indicate the positions of the upward- and downward-facing ADCPs on the mooring and the colors correspond to the location.

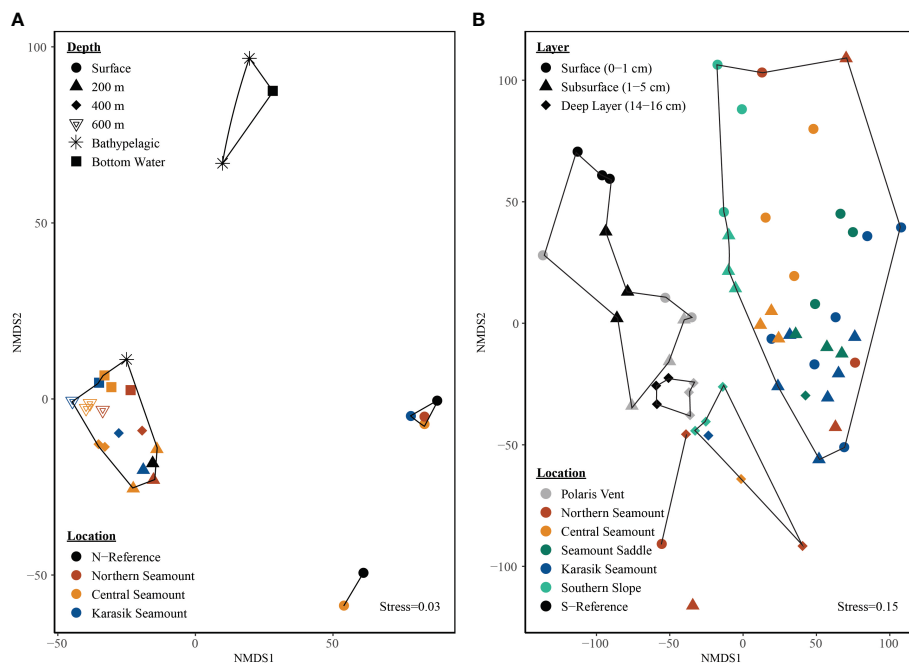


FIGURE 3 Microbial structure by location and depth along the Langseth Ridge. The non-metric multidimensional scaling (NMDS) is based on central-log transformation and euclidean distances for the (A) water column and (B) sediment-bacteria. The bottom water samples were taken at 10 m above the seafloor at each site and therefore differ in depth. Clusters represent (A) 60% dissimilarity in the water column and (B) 80% dissimilarity in the sediment.

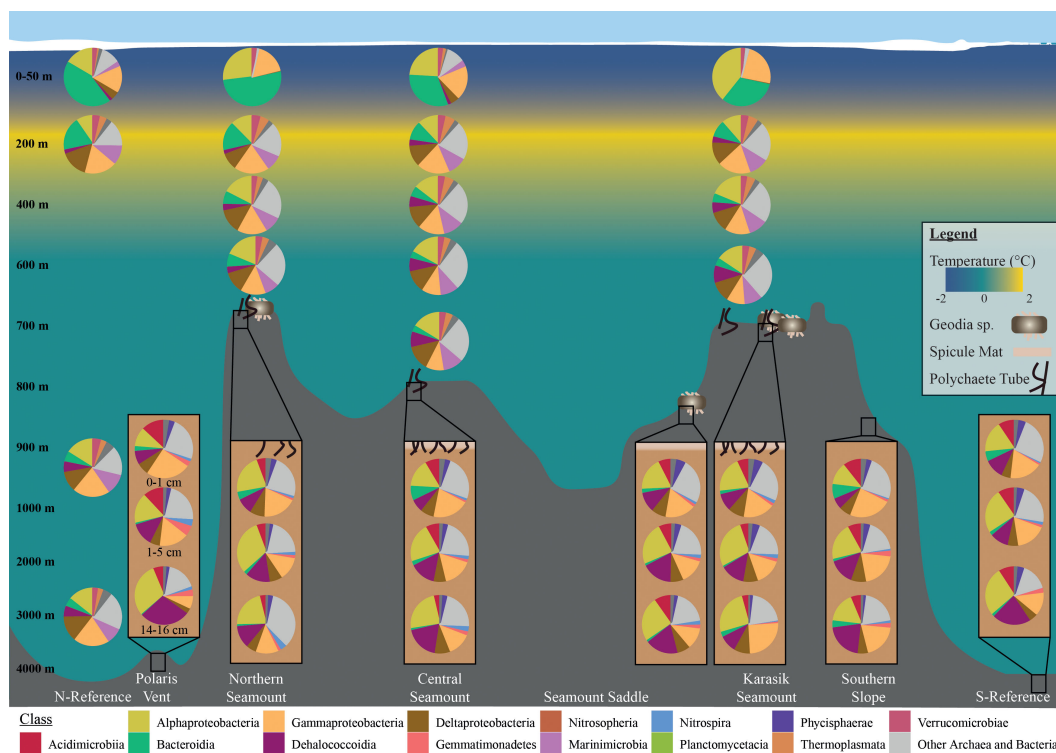


FIGURE 4 Microbial community composition along the Langseth Ridge. Relative read abundances of the top 10 classes in the water column and sediment-bacteria with the remaining grouped as “Other Archaea and Bacteria”. Average relative abundances are based on OTUs above three counts in over three percent of samples.

The pelagic microbial community was dominated by Alphaproteobacteria ~16.5%, Gammaproteobacteria ~16.2%, Bacteroidia ~12.9%, Deltaproteobacteria ~11.3%, Nitrososphaeria ~9.0% (Figure 4). To deal with the complexity of the dataset, we applied differential abundance tests at the class and genus level for all shared OTUs with absolute values higher than 1 or -1 and an adjusted p-value < 0.05. Testing the dominant classes (>1% relative abundance) showed that unclassified Marinimicrobia (0.1% vs. 6.5% respectively, log₂FC=12.5), Nitrososphaeria (0.1% vs. 8.0% respectively, log₂FC=6.0), Nitrospina (0% vs. 1.8% respectively, log₂FC=3.4), Phycisphaerae (0.2% vs. 1.7% respectively, log₂FC=2.4), Planctomycetacia (0.1% vs. 2.9% respectively, log₂FC=2.9), and Thermoplasmata (0% vs. 2.6% respectively, log₂FC=7.3) significantly increased between the 0-10 m and 50 m. The 50 m versus the cluster of 200, 400 m, 600 m, and bottom waters, we observed a significant increase in BD2-11 terrestrial group (3.4% vs. 5.6% respectively, log₂FC=2.7), Dehalococcoidia (3.4% vs. 5.6% respectively, log₂FC=5.6), unclassified Marinimicrobia (6.5% vs. 10.1%

respectively, log₂FC=12.5), Nitrospina (1.8% vs. 1.9% respectively, log₂FC=2.8), and Acidobacteria subgroup 6 (1.1% vs. 1.6% respectively, log₂FC=2.9). The cluster 200, 400 m, 600 m, and bottom waters versus the bathypelagic samples from the N-Reference showed a significant decrease in unclassified Marinimicrobia (10.1% vs. 10.0% respectively, log₂FC=-4.7) and Nitrospina (1.9% vs. 0.9% respectively, log₂FC=-5.3) as well as an increase in Dehalococcoidia (5.6% vs. 6.0% respectively, log₂FC=7.4), Phycisphaerae (1.4% vs. 2.5% respectively, log₂FC=2.7), and Planctomycetacia (3.9% vs. 2.9% respectively, log₂FC=3.9). Further testing the dominant genera (>1% relative abundance) showed that *Polaribacter 1* (27.9% vs. 1.7% respectively, log₂FC=-6.4) and SAR11 clade Ia (13.5% vs. 6.4% respectively, log₂FC=-3.4) were significantly enriched in the upper 10 m, whereas the ammonia-oxidizing archaea *Candidatus Nitrosopumilus* (0.1% vs. 7.9% respectively, log₂FC=5.2), *Nitrospina* (0% vs. 1.1% respectively, log₂FC=3.1), and Sva0996 marine group (0.1% vs. 1.0% respectively, log₂FC=2.1) became dominant in 50 m (Figures 5, S5). Comparing 50 m versus the cluster of 200 m, 400 m,

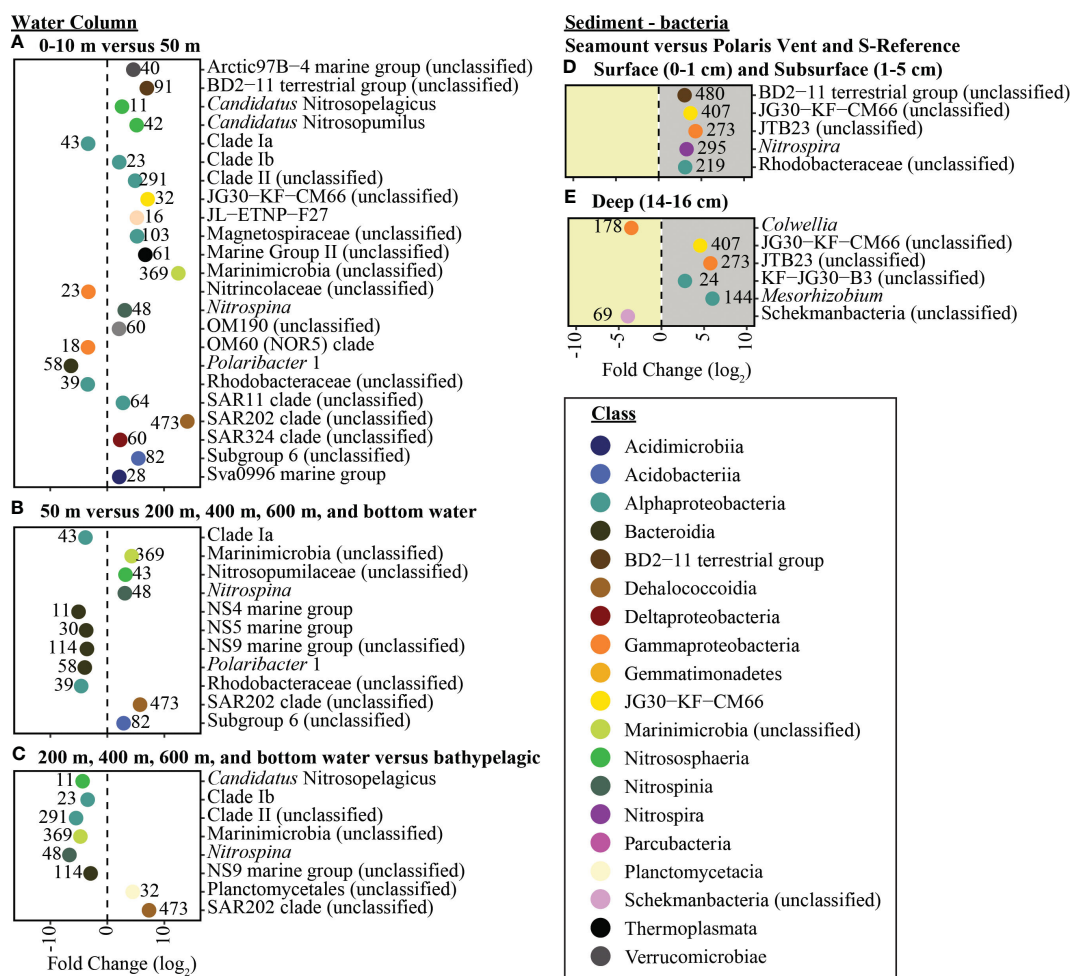


FIGURE 5
Enriched bacteria genera between sampling depths. In the water column the taxonomic enrichment analysis was performed between (A) Surface (0-10 m) and 50 m, (B) 50 m and seamount (200 m-400 m-600 m-bottom water), and (C) seamount (200 m-400 m-600 m-bottom water) and bathypelagic (2000 m-3000 m-bottom water). In the sediment the taxonomic enrichment analysis was performed between the seamount versus the Polaris Vent and S-Reference in (D) surface and subsurface sediments and (E) deep sediments. Each point represents the log₂fold change of each statistically significant genus (adjusted p-value < 0.05) with the color corresponding to the taxonomic classes and the number associated with each point represents the number of OTUs in the genus.

600 m, and bottom waters showed that NS4 and NS5 marine groups decreased (~1.5% vs. <0.6% respectively, $\log_2FC < -3.7$), while *Nitrospina* increased slightly (1.1% vs. 1.4% respectively, $\log_2FC = 3.1$; **Figure 5**). The cluster 200, 400 m, 600 m, and bottom waters versus the bathypelagic samples from the N-Reference showed a significant decrease in ammonia-oxidizing archaea *Candidatus Nitrosopelagicus* (1% vs. 0% respectively, $\log_2FC = -4.3$), *Nitrospina* (1.4% vs. 0% respectively, $\log_2FC = -6.7$), and SAR11 clade Ib (2.0% vs. 1.1% respectively, $\log_2FC = -3.5$; **Figure 5**).

3.2 Sediment

3.2.1 Sediment and porewater biogeochemistry

The sediment cores occasionally had centimeter-thick biological debris overlaying the sand that consisted of sponge spicules and polychaete worms (**Table S2**). Given the variability in substrate type and thickness, we tested whether the CPE and organic matter concentration varied across the Langseth Ridge. CPE ranged from 0.02 and 1.66 $\mu\text{g mL}^{-1}$ (n=107) and did not differ across the Langseth Ridge (**Figure 6A**). CPE significantly decreased with sediment depth in the 16 cm core replicates remaining close to the detection limit in almost all the samples (ANOVA $F_{(8,28)} = 9.28$;

$p < 0.0001$). As a derivative of CPE, chl-*a* showed similar trends with depth and usually contributed around 12% to the total CPE pool, except at S-Reference (PS101/061) with contributions that were up to 100% (**Figures 6B–D**). In contrast, TOC contents ranged from 0.40 to 12.02 $\mu\text{g mg}^{-1}$ (n=107) and TON contents from 0.11 to 1.38 $\mu\text{g mg}^{-1}$ (n=107) decreased with sediment depth and varied across the Langseth Ridge (**Figures 6E, F**). Additionally, C/N ratios ranged between 3 and 16 and significantly decreased with sediment depth at all stations (ANOVA $F_{(8,28)} = 4.25$; $p = 0.002$). C/N were highest at the Polaris Vent (e.g., PS101/140-1A) and S-Reference (e.g., PS101/061-1) (ANOVA $F_{(2,18)} = 26.72$; $p < 0.0001$; **Figure 6G**)

Porewater profiles generally showed near-constant concentrations with sediment depth, with some exceptions. DIC ranged from 1.90 to 2.75 mmol L^{-1} (n=94; **Figure 7A**), TA ranged from 1.95 to 2.93 mmol L^{-1} (n=94; **Figure 7B**), and NH_4^+ ranged from below the detection limit to 7.1 $\mu\text{mol L}^{-1}$ (n=94; **Figure 7C**) showed near-constant concentration with sediment depth except for the S-Reference, where a distinct increase of these constituents was observed. NO_3^- concentrations stayed near constant with sediment depth, except for the Polaris Vent (PS101/140-1A) where concentrations ranged from 6.04 to 15.15 $\mu\text{mol L}^{-1}$ (n=13; **Figure 7D**) and showed a distinct decrease in NO_3^- with sediment depth. PO_4^{3-} concentrations ranged between 0.11 and 0.98 $\mu\text{mol L}^{-1}$

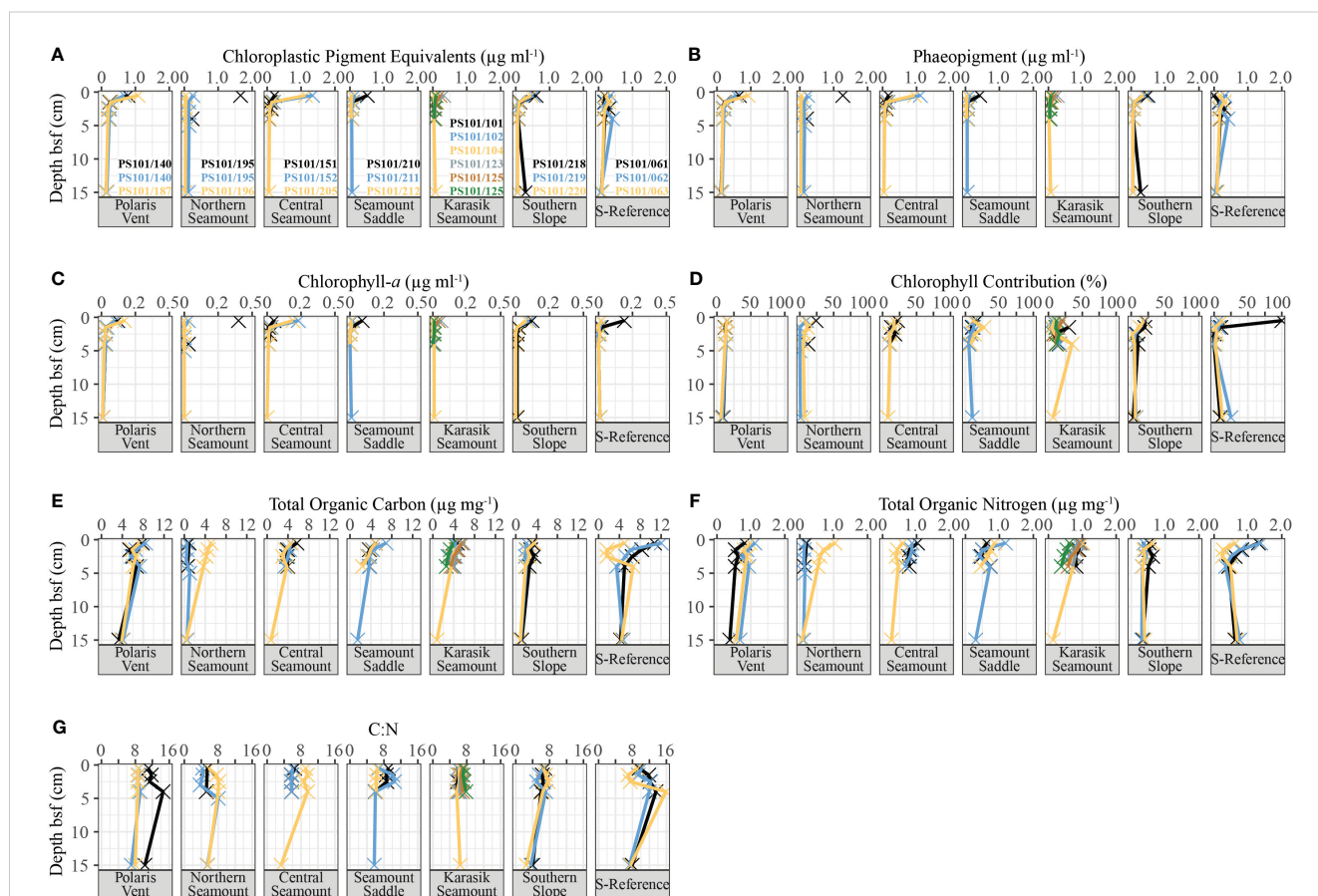


FIGURE 6 Pigment and organic matter concentrations in the sediment along the Langseth Ridge. The (A) chloroplasic Pigment equivalents (CPE) were differentiated into (B) phaeopigment and (C) chlorophyll-*a* resulting in the (D) relative chlorophyll-*a* contribution for all sediment cores. The (E) total organic carbon (TOC) and (F) total organic nitrogen (TON) were used to calculate the (G) C:N ratio. The colors correspond to the three to six biological replicate cores from each location are specified in (A) but applicable for a-g.

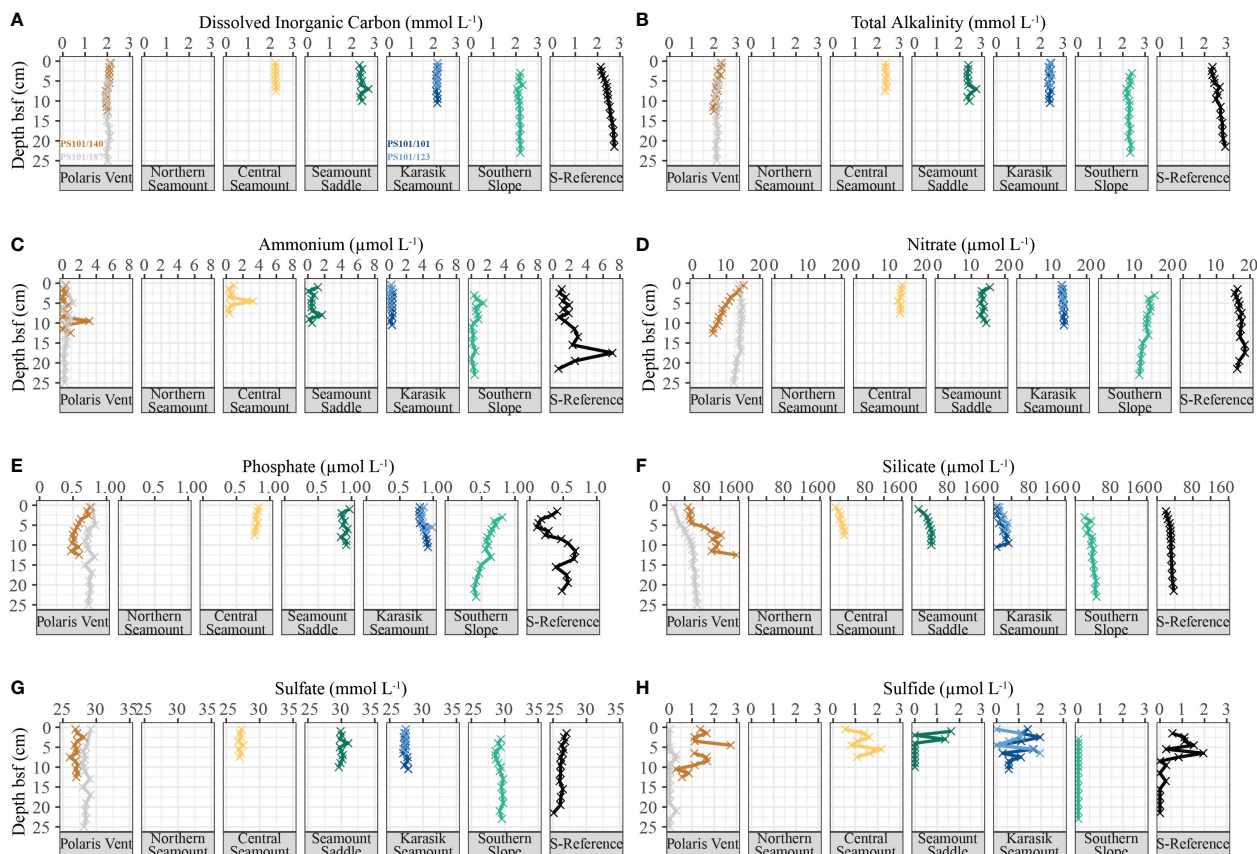


FIGURE 7
Porewater concentrations in the sediment along the Langseth Ridge. The (A) dissolved inorganic carbon, (B) total alkalinity, (C) ammonium, (D) nitrate, (E) phosphate, (F) silicate, (G) sulfate, and (H) sulfide were collected at one or two biological replicate cores from each location. The colors correspond to the biological replicates are specified in (A) but applicable for a-h. Porewater data is not available for the Northern Seamount.

(n=94; Figure 7E) and showed near-constant concentrations at most stations, while the S-Reference exhibits downcore variability. SiO₄ concentrations ranged from 6.55 to 156.06 μmol L⁻¹ (n=94; Figure 7F) and gently increased up to a plateau at all sites, except for the Polaris Vent (PS101/140-1A) that showed a steeper increase in concentrations. Sulfate concentrations ranged from 25.09 and 31.02 mmol L⁻¹ (n=94; Figure 7G) and fluctuated at all sites without any distinct trends. Similarly, sulfide concentrations ranged from below the detection limit to 3.03 μmol L⁻¹ (n=94; Figure 7H) and showed no clear trends along the seamount cluster.

3.2.2 Benthic microbial community

The microbial community of the sediment was targeted by the bacterial primer (v3v4) and an archaeal primer (v3v5). The observed richness and evenness within those OTU detected with the bacterial primer were highest in the surface sediment (Figures S3, S4). The observed richness and evenness of OTU detected with the archaeal primer were highest in the surface and subsurface sediments (Figures S3, S4). The NMDS ordination plot, based on the euclidean distance matrix of central-log transformed bacterial data, with 80% dissimilarity clusters suggests that the bacterial community clustered by location and depth (Figure 3B). The bacterial community was significantly different by location

between the seamount versus Polaris Vent (PS101/140-1 and PS101/187-1) and S-Reference (ANOSIM R=0.54 p=0.001) but also surface (0-1 cm) and subsurface (1-5 cm) versus deep layer (14-16 cm; R=0.17 p=0.001) that could be even further differentiated by nesting the substrate into sediment layer (ANOVA F_(8,61)=3.16; p<0.001). For example, Northern Seamount cores PS101/195-1A consisting of sand clustered separately from PS101/196 covered by polychaete worms in close proximity to surface and subsurface samples that were also covered by biological debris. The NMDS, based on the euclidean distance matrix of central-log transformed archaeal data, with 80% dissimilarity clusters also suggests that the archaeal community clustered by location and depth (Figure S6). The archaeal community was significantly different by location between seamount versus Polaris Vent (PS101/140-1 and PS101/187-1) and S-Reference (ANOSIM R=0.61 p=0.001) and sediment layer (ANOSIM R=0.17 p=0.002) that could be further differentiated by nesting substrate into layer since the surface and subsurface sediment layers while the deep layer clustered separately regardless of substrate (ANOVA F_(11,58)=3.87; p<0.001).

The benthic bacterial community was dominated by Alphaproteobacteria ~21.5%, Gammaproteobacteria ~16.0%, Dehalococcoidia ~15.5, Acidimicrobiia ~7.5%, and Deltaproteobacteria

~6.2% (> 60% OTU; Figures 4, S5). To deal with the complexity of the dataset, we applied differential abundance tests at the class and genus level for all shared OTUs with absolute values higher than 1 or -1 and an adjusted p-value < 0.05. Testing the dominant classes (>1% relative abundance) showed that BD2-11 terrestrial group (1.1% vs. 2.2% respectively, $\log_2FC=3.04$), JG30-KF-CM66 (1.0% vs. 2.4% respectively, $\log_2FC=3.72$), and Nitrospira (1.6% vs. 1.9% respectively, $\log_2FC=3.90$) significantly changed between the seamount versus Polaris Vent (PS101/140-1 and PS101/187-1) and S-Reference in the surface and subsurface sediments. In the deep sediment layer, Bacilli (2.5% vs. 0.1% respectively, $\log_2FC=3.54$), JG30-KF-CM66 (1.1% vs. 2.0% respectively, $\log_2FC=4.55$), Nitrospira (2.2% vs. 0.9% respectively, $\log_2FC=2.72$), and unclassified Schekmanbacteria (1.6% vs. 0.5% respectively, $\log_2FC=3.93$) significantly changed between the seamount versus Polaris Vent and S-Reference. Further testing the dominant genera (>1% relative abundance) showed that three unclassified groups and Nitrospira (1.6% vs. 1.8% $\log_2FC=3.27$) significantly changed between the seamount versus Polaris Vent and S-Reference in the surface and subsurface sediments (Figures 5, S5). In the deep sediment layer, four unclassified groups, Colwellia (1.5% vs. 0% respectively, $\log_2FC=-3.53$), and Mesorhizobium (0.1% vs. 6.4% respectively, $\log_2FC=5.99$) significantly changed between the seamount versus Polaris Vent and S-Reference (Figures 5, S5). Since seamounts can select for chemolithotrophic bacteria, we specifically screened for Arcobacter, Sulfurimonas, and Sulfurovum but these genera were <0.1% read abundance in the surface sediments, <0.3% read abundance in subsurface samples, and < 0.01% read abundance in the deep sediment layers, therefore not contributing to the dominant community.

The benthic archaeal community was dominated by Nitrososphaeria (formerly MG-1) and Woesearchaeia. Additionally, taxa in the low abundance fraction included Marine Benthic Group A, Iainarchaeia, Nanohaloarchaeia, Thermococci, and Thermoplasmata. The differential abundance tests did not identify any significant differences between any set of our samples, possibly due to the dominance of Nitrososphaeria.

3.2.3 Environmental drivers of the microbial community in the sediment

Incorporating the metadata, porewater, and sediment biogeochemistry in the analysis allowed us to determine the sources of variation between groups. For both bacteria and archaea, the layer-nested-substrate was the primary source of variation, explaining 17% of differences between groups (PERMANOVA, $p < 0.001$; Table S3). The biogeochemistry explained part of the variability in the benthic microbial community. In the surface sediments (0-1 cm), CPE was the single environmental variable with the most explanatory power and explained up to 8% of the variability in the bacterial community, while it explained 11% of the variability in the archaeal community structure (Table S4). TOC explained up to 6% of the variance in the bacterial and 8% in the archaeal community structure (Figure S7, Table S4). Furthermore, “location” and “substrate” both explained between 16% and 19% of the group variation (PERMANOVA, $p < 0.001$; Table S5).

4 Discussion

4.1 Pelagic microbes in the Central Arctic Ocean

In the fall of 2016, sea ice reached one of the lowest minimum extents with only 4.17 million km² (NSIDC, 2022) but covered the Langseth Ridge and contributed to the stratified water column (Figures 2A, B). The epipelagic communities were enriched in Alphaproteobacteria and Bacteroidia, particularly, the genus Polaribacter that has been tightly associated with phytoplankton bloom dynamics in the Arctic (Wilson et al., 2017 Fadeev et al., 2021; Wietz et al., 2021; von Jackowski et al., 2022). Yet, we measure a fluorescence below 0.13 mg m⁻³ and Boetius (2016) reported low abundances of phytoplankton in the surface waters, including Melosira arctica a species that can significantly alter the magnitude and composition of organic matter seafloor (Ambrose et al., 2005; Boetius et al., 2013). Additionally, Boetius (2016) reported high abundances of zooplankton, which indicate post-bloom conditions in September. Albeit the absence of a bloom to locally exudate organic substrates, 75% of the organic matter in the central Arctic Ocean can originate from inflowing Atlantic Water and could continue to supply microbes in the epipelagic waters well after the productive season has ended (Piontek et al., 2021). Compared to the epipelagic waters, the meso- and bathypelagic waters increased in richness and evenness, enriched in Proteobacteria and archaea like Nitrososphaeria. The high degree of similarity in the microbial community between 200 m, 400 m, and 600 m (Figures 3, 4) along with slow currents suggest that recirculating water masses do not significantly alter the bacterial community. In general, there are very few datasets on pelagic microbial communities (e.g., Rapp et al., 2018, this study) or standing stocks (e.g., Nöthig et al., 2020a; Nöthig et al., 2020b) from the central Arctic Ocean. The lack of data is directly tied to the logistical barriers associated with high Arctic research and make any observations highly valuable, especially in light of the potential system changes associated with climate change.

4.2 Exploring the drivers of pelagic-benthic coupling

Seamounts have the potential to modify the hydrodynamic processes within the water column, but the slow currents and pelagic microbial community are not indicative of seamount-specific circulation dynamics at the Langseth Ridge. Theoretically, the Langseth Ridge could generate a Taylor cap according to the calculated Rossby number of 0.07 and a fractional height of 0.8 for Langseth Ridge (Chapman and Haidvogel, 1992). A Taylor cap would generate an anticyclonic gyre and isolate the flow at the seamount (Chapman and Haidvogel, 1992). Despite this theoretical potential, the current velocities at the Langseth Ridge are approximately 10 cm s⁻¹ and resemble those rather sluggish currents typical of the central Arctic Ocean (Woodgate et al., 2001; Nikolopoulos et al., 2009; Håvik et al., 2017). In contrast,

current velocities at those seamounts with locally enhanced matter fluxes can approach 35 cm s^{-1} or more (Dower et al., 1992; Mouriño et al., 2001; Wilson and Boehlert, 2004; Mohn et al., 2013). Additionally, the net westward flow and accelerations at local seamount summits, such as the Northern Seamount (Figure 2), do not suggest a circulating current around the ridge. Instead, the net westward flow appears to be responsible for fast-core erosion at the Northern Seamount and slow-core erosion at the Southern Slope (Hernández-Molina et al., 2006), while depositional trails are created on the western flank of the ridge based on the bathymetry (Figure 1).

The seamount topography did not affect the pelagic microbial community but dense aggregations of large sponges might contribute to the pelagic-benthic coupling of microbes. The water column was shaped by the common pelagic groups in midwater communities including Proteobacteria, particularly SAR11 cluster representatives, Marinimicrobia, and Nitrososphaeria. Although the composition wasn't significantly different between stations, we observed differences in microbial richness (Figure S4). The richness was lower in the bottom waters compared to 600 m at the Northern Seamount and Central Seamount where we observed sponges using the TV-MUC (Table S2), while the richness was higher in the bottom waters compared to 600 m at the northern flank of the Karasik Seamount and N-Reference where sponges could not be observed. The decreased richness in the bottom waters could be due to the dense *Geodiia* sp. sponge grounds (Morganti et al., 2021; Morganti et al., 2022), similar to observations at Schulz Bank seamount (Roberts et al., 2018; Meyer et al., 2019; Busch et al., 2020). Sponges, including *Geodiia* sp., are efficient filter feeders that can move large volumes of water and retain particles, microbes, and dissolved organic matter (Reiswig, 1971a; Reiswig, 1971b; Vogel, 1977; Frost, 1980; Willenz et al., 1986; Maldonado et al., 2012; Tjensvoll et al., 2013; Soetaert et al., 2016). Our data suggests that benthic-pelagic coupling mediated by sponges on pelagic microbes might explain the slightly reduced microbial richness of the water residing above sponge grounds in the central Arctic along Langseth Ridge (McMurray et al., 2016; Van Oevelen et al., 2018; Busch et al., 2020).

4.3 Benthic microbial diversity on inactive Arctic seamounts

The substrate variability from bare sand to centimeter-thick biological debris likely explains the range of TOC and TON contents across the Langseth Ridge. Sponge locomotion left centimeter-thick spicule mats (Morganti et al., 2021; Morganti et al., 2022) that trapped polychaete tubes shielding the benthic microbes from potential sinking organic matter. The decreasing TOC and TON contents with sediment depth would support microbially mediated active organic matter degradation along the Langseth Ridge and at S-Reference, but the near-constant porewater profiles of the degradation products DIC, TA, and NH_4^+ suggest limited microbial activity in the sediment at Langseth Ridge sites.

Given that dissolved NO_3^- is utilized by microbes during redox processes, near-constant or only gently increasing NO_3^- concentration profiles further imply low microbial activity. Therefore, the solid phase and porewater contradict each other. If we hypothesize that low sedimentation rates due to a limited pelagic biological production and slow burial rates as a consequence of the sponge spicule mats acting as a physical barrier, then increased residence time of the organic matter would result in gently decreasing concentrations in the solid phase profiles over long-time scales. We strongly encourage future research to investigate the solid phase and porewater profiles under ice-covered conditions in Arctic sediments.

Although the sponge spicule mats act as a barrier for phytoplankton-derived organic matter, the spicules might provide sponge-derived chitin and proteinaceous matter to the microbial community in the surface sediments. A taxon with the potential to grow on proteinaceous matter from organic remnants in oxygenated deep-sea sediments are *Woeseia* (Figure S5) (Hoffmann et al., 2020). *Woeseia* has the genomic repertoire to catabolize putative peptidases and cycle detrital proteins in sediments (Hoffmann et al., 2020). However, *Woeseia* has a high functional variability and has been widely observed within deep sea sediments (Mußmann et al., 2017; Meier et al., 2019; Soltwedel et al., 2023). To fully understand the degree of influence the biological debris has on the microbial community, future research should focus on the interactions between sediments and sponges (e.g., Busch et al., 2020). Sponges, especially those in polar regions, host a low diversity of sponge-specific microbes that may be similar to those detected in sea ice or sediments (Webster et al., 2004; Pape et al., 2006).

Aside from the possible sponge-derived matter degradation, the benthic microbial communities at the Langseth Ridge resemble taxa associated with deep sea sediments like Alphaproteobacteria, Gammaproteobacteria, Acidimicrobia, Dehalococcoidia, and Nitrospira (Cerqueira et al., 2015; Zhang et al., 2015; Zhang et al., 2016; Adam et al., 2019; Varliero et al., 2019). Additionally, Nitrososphaeria is an abundant member in marine sediments (Wuchter et al., 2006; Roussel et al., 2009; Durbin and Teske, 2010) and in Arctic sediments (Park et al., 2012; Pester et al., 2012). Thus, these findings indicate that Langseth Ridge sediment communities reflect typical heterotrophic communities present in the deep sea of oligotrophic ocean biomes in the absence of proximal hydrothermal activity. If the Langseth Ridge seamounts were hydrothermally active, we would expect mesophilic *Epsilonproteobacteria*, thermophilic *Aquificales*, and archaea to contribute to the dominant fraction of the microbial community (Teske et al., 2002; López-García et al., 2003; Nakagawa et al., 2005; Wei et al., 2013; Teske et al., 2014; Cerqueira et al., 2015; Cerqueira et al., 2017; Meier et al., 2017; Møller et al., 2018). Instead, *Epsilonproteobacteria* contribute to the rare fraction of the microbial community in the deepest sediment layer. The only station to suggest some degree of suboxic and potentially advective flux was the Polaris Vent (PS101/140-1A) but without any significant shift in the microbial community.

5 Conclusion

Our study explores the hydrodynamics with ties to the pelagic-benthic coupling of the microbial community in the context of sediment geochemistry at a seamount cluster with three individual peaks in the central Arctic Ocean. The water column was stratified from the N-Reference across the Langseth Ridge and towards the S-Reference, characterized by common pelagic microbes and slow current dynamics that were not influenced by the topography of the seamounts. The seamounts were covered in giant sponge grounds that influence the microbial diversity in bottom water and suggest that the sponges might play a role in pelagic-benthic coupling at the Langseth Ridge. Simultaneously, the dense sponge spicule mats covered the sediment and reduced the availability of settling phytodetritus but possibly acted as a source of other trophic resources (e.g., refractory protein and chitin) amidst a typical microbial community in the deep sea of oligotrophic ocean biomes. We observed dead tube worms inside the upper few centimeters of the sediment cores and combined with the absence of hydrothermal-indicator microbes, e.g., *Epsilonproteobacteria*, suggest that the Langseth Ridge had no active hydrothermal activity at the time of sampling, whereas it may have had in the past. Overall, these findings expand our current knowledge about the effect of inactive seamounts on microbial community dynamics all the while stimulating future research to explore the deep sea biodiversity and ecosystem functioning of polar regions.

Data availability statement

The datasets presented in this study can be found in online repositories. The names of the repository/repositories and accession number(s) can be found below: <https://www.ebi.ac.uk/ena>, PRJEB34976. <https://doi.pangaea.de/10.1594/PANGAEA.904373>; <https://doi.pangaea.de/10.1594/PANGAEA.871927>; <https://doi.pangaea.de/10.1594/PANGAEA.910048>.

Author contributions

AvJ, PB, and MM designed the study. AvJ organized the data for public repositories, performed the statistical analysis, and wrote the manuscript with sections from MW and TS. All authors contributed to the revisions and approved the submitted version.

Funding

Funding was provided by the ERC Advanced Investigator Grant ABYSS (294757) to Antje Boetius. Additional funding came from the Helmholtz Association, the German Research Foundation

(DFG), and the Max Planck Society (MPG). AvJ was funded by the International-Max-Planck-Research-Schools Scholarship. MW received funding from the DFG Cluster of Excellence “The Ocean in the Earth System” via incentive grant “Hydrothermal plumes at the ultraslow-spreading Gakkel Ridge, Karasik Seamount”. PB was supported by the HGF Infrastructure Program FRAM of the Alfred Wegener Institute Helmholtz Centre for Polar and Marine Research. MM was supported by the German Ministry of Research and Education (BMBF grant no. 03F0707A-G) as part of the Mining Impact project of the Joint Programming Initiative of Healthy and Productive Seas and Oceans (JPIOceans).

Acknowledgments

We thank Prof. Dr. Antje Boetius for supporting this study and for suggestions on the manuscript. Thank you to the captain and crew of the *RV Polarstern* for assisting with the sample acquisition. We would also like to thank Dr. Halina Tegetmeyer for support with Illumina sequencing (CeBiTec laboratory), Jana Bäger and Jakob Barz for the onboard sample collection, and Autun Purser for supplying the videos of the TV-MUC deployments. Thank you to our colleagues in the Deep Sea Ecology and Technology Max Planck Institute for Marine Microbiology and Alfred Wegener Institute for Polar and Marine Research bridge group. We thank the two anonymous reviewers for their helpful suggestions in improving the manuscript.

Conflict of interest

The authors declare that the research was conducted in the absence of any commercial or financial relationships that could be construed as a potential conflict of interest.

Publisher's note

All claims expressed in this article are solely those of the authors and do not necessarily represent those of their affiliated organizations, or those of the publisher, the editors and the reviewers. Any product that may be evaluated in this article, or claim that may be made by its manufacturer, is not guaranteed or endorsed by the publisher.

Supplementary material

The Supplementary Material for this article can be found online at: <https://www.frontiersin.org/articles/10.3389/fmars.2023.1216442/full#supplementary-material>

References

- Adam, N., Kriete, C., Garbe-Schoöenberg, D., Gonnella, G., Krause, S., Schippers, A., et al. (2019). Microbial community compositions and geochemistry of sediments with increasing distance to the hydrothermal vent outlet in the kairei field. *Geomicrobiol. J.* 37, 242–254. doi: 10.1080/01490451.2019.1694107
- Amann, R. I., Krumholz, L., and Stahl, D. A. (1990). Fluorescent-oligonucleotide probing of whole cells for determinative, phylogenetic, and environmental studies in microbiology. *J. Bacteriol.* 172, 762–770. doi: 10.1128/JB.172.2.762-770.1990
- Ambrose, W. G., Von Quillfeldt, C., Clough, L. M., Tilney, P. V. R., and Tucker, T. (2005). The sub-ice algal community in the Chukchi sea: Large- and small-scale patterns of abundance based on images from a remotely operated vehicle. *Polar Biol.* 28, 784–795. doi: 10.1007/s00300-005-0002-8
- Beckmann, A., and Mohn, C. (2002). The upper ocean circulation at Great Meteor Seamount. *Ocean Dyn.* 52, 179–193. doi: 10.1007/s10236-002-0017-4
- Benjamini, Y., and Hochberg, Y. (1995). Controlling the false discovery rate: A practical and powerful approach to multiple testing. *J. R. Stat. Soc. Ser. B* 57, 289–300. doi: 10.1111/j.2517-6161.1995.tb02031.x
- Böer, S. I., Hedtkamp, S. I. C., Van Beusekom, J. E. E., Fuhrman, J. A., Boetius, A., and Ramette, A. (2009). Time- and sediment depth-related variations in bacterial diversity and community structure in subtidal sands. *ISME J.* 3, 780–791. doi: 10.1038/ismej.2009.29
- Boetius, A. (2016). *PS101 weekly report no. 1*. (Bremerhaven, Germany: Alfred Wegener Institute, Helmholtz Centre for Polar and Marine Research)
- Boetius, A., Albrecht, S., Bakker, K., Bienhold, C., Felden, J., Fernandez-Mendez, M., et al. (2013). Export of algal biomass from the melting arctic sea ice. *Science* 339, 1430–1432. doi: 10.1126/science.1231346
- Boetius, A., and Purser, A. (2017). *The expedition PS101 of the research vessel POLARSTERN to the arctic ocean in 2016*. (Bremerhaven, Germany: Alfred Wegener Institute, Helmholtz Centre for Polar and Marine Research). doi: 10.2312/BzPM_0706_2017
- Bolger, A. M., Lohse, M., and Usadel, B. (2014). Trimmomatic: A flexible trimmer for Illumina sequence data. *Bioinformatics* 30, 2114–2120. doi: 10.1093/bioinformatics/btu170
- Brozna, J. M., Childers, V. A., Lawver, L. A., Gahagan, L. M., Forsberg, R., Faleide, J. I., et al. (2003). New aerogeophysical study of the Eurasia Basin and Lomonosov Ridge: Implications for basin development. *Geology* 31, 825–828. doi: 10.1130/G19528.1
- Busch, K., Hanz, U., Mienis, F., Mueller, B., Franke, A., Martyn Roberts, E., et al. (2020). On giant shoulders: How a seamount affects the microbial community composition of seawater and sponges. *Biogeosciences* 17, 3471–3486. doi: 10.5194/bg-17-3471-2020
- Carqueira, T., Pinho, D., Egas, C., Froufe, H., Altermark, B., Candeias, C., et al. (2015). Microbial diversity in deep-sea sediments from the Menez Gwen hydrothermal vent system of the Mid-Atlantic Ridge. *Mar. Genomics* 24, 343–355. doi: 10.1016/j.margen.2015.09.001
- Carqueira, T., Pinho, D., Froufe, H., Santos, R. S., Bettencourt, R., and Egas, C. (2017). Sediment microbial diversity of three deep-sea hydrothermal vents southwest of the azores. *Microb. Ecol.* 74, 332–349. doi: 10.1007/s00248-017-0943-9
- Chapman, D. C., and Haidvogel, D. B. (1992). Formation of Taylor caps over a tall isolated seamount in a stratified ocean. *Geophys. Astrophys. Fluid Dyn.* 65, 31–65. doi: 10.1080/03091929208228084
- Cline, J. (1969). Spectrophotometric determination of hydrogen sulfide in natural waters. *Limnol. Oceanogr.* 14, 454–458. doi: 10.4319/lo.1969.14.3.0454
- Cochran, J. R. (2008). Seamount volcanism along the Gakkel Ridge, Arctic Ocean. *Geophys. J. Int.* 174, 1153–1173. doi: 10.1111/j.1365-246X.2008.03860.x
- Cochran, J. R., Kurras, G. J., Edwards, M. H., and Coakley, B. J. (2003). The Gakkel Ridge: Bathymetry, gravity anomalies, and crustal accretion at extremely slow spreading rates. *J. Geophys. Res. Solid Earth* 108, 1–22. doi: 10.1029/2002JB001830
- Consalvey, M., Clark, M. R., Rowden, A. A., and Stocks, K. I. (2010). “Life on seamounts,” in *Life in the world's oceans* (Oxford, UK: Wiley-Blackwell), 123–138. doi: 10.1002/9781444325508.ch7
- DeMets, C., Gordon, R. G., Argus, D. F., and Stein, S. (1994). Effect of recent revisions to the geomagnetic reversal time scale on estimates of current plate motions. *Geophys. Res. Lett.* 21, 2191–2194. doi: 10.1029/94GL02118
- Dickson, A. G. (1981). An exact definition of total alkalinity and a procedure for the estimation of alkalinity and total inorganic carbon from titration data. *Deep Sea Res. Part A Oceanogr. Res. Pap.* 28, 609–623. doi: 10.1016/0198-0149(81)90121-7
- Diepenbroek, M., Glöckner, F. O. F. O., Grobe, P., Güntsch, A., Huber, R., König-Ries, B., et al. (2014). Towards an integrated biodiversity and ecological research data management and archiving platform: The German federation for the curation of biological data (GFBio). *Inform.* 2014, 1711–1721.
- Djurhuus, A., Boersch-Supan, P. H., Mikalsen, S.-O., and Rogers, A. D. (2017a). Microbe biogeography tracks water masses in a dynamic oceanic frontal system. *R. Soc. Open Sci.* 4, 170033. doi: 10.1098/rsos.170033
- Djurhuus, A., Read, J. F., and Rogers, A. D. (2017b). The spatial distribution of particulate organic carbon and microorganisms on seamounts of the South West Indian Ridge. *Deep. Res. Part II Top. Stud. Oceanogr.* 136, 73–84. doi: 10.1016/j.dsr2.2015.11.015
- Dower, J., Freeland, H., and Juniper, K. (1992). A strong biological response to oceanic flow past Cobb Seamount. *Deep Sea Res. Part A Oceanogr. Res. Pap.* 39, 1139–1145. doi: 10.1016/0198-0149(92)90061-W
- Dower, J. F., and Mackas, D. L. (1996). “Seamount effects” in the zooplankton community near Cobb Seamount. *Deep. Res. Part I Oceanogr. Res. Pap.* 43, 837–858. doi: 10.1016/0967-0637(96)00040-4
- Durbin, A. M., and Teske, A. (2010). Sediment-associated microdiversity within the Marine Group I Crenarchaeota. *Environ. Microbiol. Rep.* 2, 693–703. doi: 10.1111/j.1758-2229.2010.00163.x
- Emerson, D., and Moyer, C. L. (2010). Microbiology of seamounts. *Oceanography* 23, 148–163. doi: 10.5670/oceanog.2010.67
- Fadeev, E. (2018). *Bact-comm-PS85*. Available at: <https://github.com/edfadeev/Bact-comm-PS85>.
- Fadeev, E., Wietz, M., von Appen, W. J., Iversen, M. H., Nöthig, E. M., Engel, A., et al. (2021). Submesoscale physicochemical dynamics directly shape bacterioplankton community structure in space and time. *Limnol. Oceanogr.* 66, 2901–2913. doi: 10.1101/2020.09.02.279232
- Fisher, A. T. (2010). and wheat, C Seamounts as conduits for massive fluid, heat, and solute fluxes on ridge flanks. *G. Oceanography* 23, 74–87. doi: 10.5670/oceanog.2010.63
- Frost, T. M. (1980). Clearance rate determinations for the freshwater sponge *Spongilla lacustris*: effects of temperature, particle type and concentration, and sponge size. *Arch. fuer Hydrobiol.* 90, 330–356.
- Genin, A., Dayton, P. K., Lonsdale, P. F., and Spiess, F. N. (1986). Corals on seamount peaks provide evidence of current acceleration over deep-sea topography. *Nature* 322, 59–61. doi: 10.1038/322059a0
- Hansen, H. P., and Koroleff, F. (2007). Determination of nutrients. In *Methods of Seawater Analysis*. (Weinheim, Germany), 159–228. doi: 10.1002/9783527613984.ch10
- Harris, R. N., Fisher, A. T., and Chapman, D. S. (2004). Fluid flow through seamounts and implications for global mass fluxes. *Geology* 32, 725–728. doi: 10.1130/G20387.1
- Hassenrück, C., Fink, A., Lichtschlag, A., Tegetmeyer, H. E., De Beer, D., and Ramette, A. (2016). Quantification of the effects of ocean acidification on sediment microbial communities in the environment: The importance of ecosystem approaches. *FEMS Microbiol. Ecol.* 92, 1–12. doi: 10.1093/femsec/fiw027
- Håvik, L., Pickart, R. S., Våge, K., Torres, D., Thurnherr, A. M., Beszczynska-Möller, A., et al. (2017). Evolution of the East Greenland Current from Fram Strait to Denmark Strait: Synoptic measurements from summer 2012. *J. Geophys. Res. Ocean.* 122, 1974–1994. doi: 10.1002/2016JC012228
- Hernández-Molina, F. J., Larter, R. D., Rebecco, M., and Maldonado, A. (2006). Miocene reversal of bottom water flow along the Pacific Margin of the Antarctic Peninsula: Stratigraphic evidence from a contourite sedimentary tail. *Mar. Geol.* 228 (1–4), 93–116. doi: 10.1016/j.margeo.2005.12.010
- Hoffmann, K., Bienhold, C., Buttigieg, P. L., Knittel, K., Laso-Pérez, R., Rapp, J. Z., et al. (2020). Diversity and metabolism of Woeseiales bacteria, global members of marine sediment communities. *ISMEJ.* 14, 1042–1056. doi: 10.1038/s41396-020-0588-4
- Karasik, A. M. (1968). Magnetic anomalies of the Gakkel Ridge and origin of the Eurasia Subbasin of the Arctic Ocean. *Geophys. Methods Prospect Arct.* 5, 9–19.
- Kirsten, W. J. (1979). Automatic methods for the simultaneous determination of carbon, hydrogen, nitrogen, and sulfur, and for sulfur alone in organic and inorganic materials. *Anal. Chem.* 51, 1173–1179. doi: 10.1021/ac50044a019
- Kitchingman, A., and Lai, S. (2004). “Inferences on potential seamount locations from mid-resolution bathymetric data,” in *Seamounts: Biodiversity Fisheries*, 7–12.
- Klindworth, A., Pruesse, E., Schweer, T., Peplies, J., Quast, C., Horn, M., et al. (2013). Evaluation of general 16S ribosomal RNA gene PCR primers for classical and next-generation sequencing-based diversity studies. *Nucleic Acids Res.* 41, e1–e1. doi: 10.1093/nar/gks808
- Klügel, A., Villinger, H., Römer, M., Kaul, N., Krastel, S., Lenz, K. F., et al. (2020). Hydrothermal activity at a cretaceous seamount, canary archipelago, caused by rejuvenated volcanism. *Front. Mar. Sci.* 7. doi: 10.3389/fmars.2020.584571
- Lavelle, J. W., and Mohn, C. (2010). Motion, commotion, and biophysical connections at deep ocean seamounts. *Oceanography* 23, 90–103. doi: 10.5670/oceanog.2010.64
- López-García, P., Duperron, S., Philippot, P., Foriel, J., Susini, J., and Moreira, D. (2003). Bacterial diversity in hydrothermal sediment and epsilonproteobacterial dominance in experimental microcolonizers at the Mid-Atlantic Ridge. *Environ. Microbiol.* 5, 961–976. doi: 10.1046/j.1462-2920.2003.00495.x
- Lorenzen, C. (1967). Determination of chlorophyll and pheopigments: spectrophotometric equations. *Limnol. Oceanogr.* 12, 343–346. doi: 10.4319/lo.1967.12.2.0343
- Mahé, F., Rognes, T., Quince, C., de Vargas, C., and Dunthorn, M. (2014). Swarm: robust and fast clustering method for amplicon-based studies. *PeerJ* 2, e593. doi: 10.7717/peerj.593

- Maldonado, M., Ribes, M., and van Duyl, F. C. (2012). Nutrient fluxes through sponges. Biology, budgets, and ecological implications. *Adv. Mar. Biol.* 62, 113–182. doi: 10.1016/B978-0-12-394283-8.00003-5
- Martin, M. (2011). Cutadapt removes adapter sequences from high-throughput sequencing reads. *EMBNET journal* 17, 10–12. doi: 10.14806/ej.17.1.200
- McMurdie, P. J., and Holmes, S. (2013). phyloseq: An R package for reproducible interactive analysis and graphics of microbiome census data. *PLoS One* 8, 1–11. doi: 10.1371/journal.pone.0061217
- McMurray, S. E., Johnson, Z. I., Hunt, D. E., Pawlik, J. R., and Finelli, C. M. (2016). Selective feeding by the giant barrel sponge enhances foraging efficiency. *Limnol. Oceanogr.* 61, 1271–1286. doi: 10.1002/lno.10287
- Meier, D. V., Pjevac, P., Bach, W., Hourdez, S., Girguis, P. R., Vidoudez, C., et al. (2017). Niche partitioning of diverse sulfur-oxidizing bacteria at hydrothermal vents. *ISME J.* 11, 1545–1558. doi: 10.1038/ismej.2017.37
- Meier, D. V., Pjevac, P., Bach, W., Markert, S., Schweder, T., Jamieson, J., et al. (2019). Microbial metal-sulfide oxidation in inactive hydrothermal vent chimneys suggested by metagenomic and metaproteomic analyses. *Environ. Microbiol.* 21, 682–701. doi: 10.1111/1462-2920.14514
- Mendonça, A., Aristegui, J., Vilas, J. C., Montero, M. F., Ojeda, A., Espino, M., et al. (2012). Is there a seamount effect on microbial community structure and biomass? The case study of seine and sedlo seamounts (Northeast Atlantic). *PLoS One* 7, e29526. doi: 10.1371/journal.pone.0029526
- Meyer, H. K., Roberts, E. M., Rapp, H. T., and Davies, A. J. (2019). Spatial patterns of arctic sponge ground fauna and demersal fish are detectable in autonomous underwater vehicle (AUV) imagery. *Deep. Res. Part I Oceanogr. Res. Pap.* 153, 103137. doi: 10.1016/j.dsr.2019.103137
- Michael, P. J., Langmuir, C. H., Dick, H. J. B., Snow, J. E., Goldstein, S. L., Graham, D. W., et al. (2003). Magmatic and amagmatic seafloor generation at the ultraslow-spreading Gakkel ridge, Arctic Ocean. *Nature* 423, 956–961. doi: 10.1038/nature01704
- Miller, K. J., and Gunasekera, R. M. (2017). A comparison of genetic connectivity in two deep sea corals to examine whether seamounts are isolated islands or stepping stones for dispersal. *Sci. Rep.* 7, 1–14. doi: 10.1038/srep46103
- Mohn, C., Erofeeva, S., Turnewitsch, R., Christiansen, B., and White, M. (2013). Tidal and residual currents over abrupt deep-sea topography based on shipboard ADCP data and tidal model solutions for three popular bathymetry grids. *Ocean Dyn.* 63, 195–208. doi: 10.1007/s10236-013-0597-1
- Møller, M. H., Glombitza, C., Lever, M. A., Deng, L., Morono, Y., Inagaki, F., et al. (2018). D: L-Amino Acid modeling reveals fast microbial turnover of days to months in the subsurface hydrothermal sediment of Guaymas Basin. *Front. Microbiol.* 9. doi: 10.3389/fmicb.2018.00967
- Morganti, T. M., Purser, A., Rapp, H. T., German, C. R., Jakuba, M. V., Hehemann, L., et al. (2021). *In situ* observation of sponge trails suggests common sponge locomotion in the deep central Arctic. *Curr. Biol.* 31, R368–R370. doi: 10.1016/j.cub.2021.03.014
- Morganti, T. M., Slaby, B. M., de Kluijver, A., Busch, K., Hentschel, U., Middelburg, J. J., et al. (2022). Giant sponge grounds of Central Arctic seamounts are associated with extinct seep life. *Nat. Commun.* 13, 1–15. doi: 10.1038/s41467-022-28129-7
- Mouriño, B., Fernández, E., Serret, P., Harbour, D., Sinha, B., and Pingree, R. (2001). Variability and seasonality of physical and biological fields at the Great Meteor Tablemount (subtropical NE Atlantic). *Oceanol. Acta* 24, 167–185. doi: 10.1016/S0399-1784(00)01138-5
- Mußmann, M., Pjevac, P., Krüger, K., and Dykma, S. (2017). Genomic repertoire of the Woeseiaceae/ITB255, cosmopolitan and abundant core members of microbial communities in marine sediments. *ISME J.* 11, 1276–1281. doi: 10.1038/ismej.2016.185
- Nakagawa, S., Takai, K., Inagaki, F., Hirayama, H., Nunoura, T., Horikoshi, K., et al. (2005). Distribution, phylogenetic diversity and physiological characteristics of epsilon-Proteobacteria in a deep-sea hydrothermal field. *Environ. Microbiol.* 7, 1619–1632. doi: 10.1111/j.1462-2920.2005.00856.x
- Nikolopoulos, A., Pickart, R. S., Fratantoni, P. S., Shimada, K., Torres, D. J., and Jones, E. P. (2009). The western Arctic boundary current at 152°W: Structure, variability, and transport. *Deep. Res. Part II Top. Stud. Oceanogr.* 56, 1164–1181. doi: 10.1016/j.dsr2.2008.10.014
- Nöthig, E. M., Lalonde, C., Fahl, K., Metfies, K., Salter, I., and Bauerfeind, E. (2020b). Annual cycle of downward particle fluxes on each side of the Gakkel Ridge in the central Arctic Ocean: Particle fluxes in Central Arctic Ocean. *Philos. Trans. R. Soc A Math. Phys. Eng. Sci.* 378, 1–12. doi: 10.1098/rsta.2019.0368
- Nöthig, E.-M., Ramondenc, S., Haas, A., Hehemann, L., Walter, A., Bracher, A., et al. (2020a). Summertime chlorophyll a and particulate organic carbon standing stocks in surface waters of the Fram Strait and the Arctic Ocean (2015). *Front. Mar. Sci.* 7. doi: 10.3389/fmars.2020.00350
- NSIDC. (2022). Arctic sea ice minimum ties for tenth lowest. Available at: <http://nsidc.org/arcticseaicenews/2022/09/>.
- Pape, T., Hoffmann, F., Quéric, N. V., Von Juterzenka, K., Reitner, J., and Michaelis, W. (2006). Dense populations of Archaea associated with the demosponge *Tentorium semisuberites* Schmid from Arctic deep-waters. *Polar Biol.* 29, 662–667. doi: 10.1007/s00300-005-0103-4
- Parada, A. E., Needham, D. M., and Fuhrman, J. A. (2016). Every base matters: assessing small subunit rRNA primers for marine microbiomes with mock communities, time series and global field samples. *Environ. Microbiol.* 18, 1403–1414. doi: 10.1111/1462-2920.13023
- Park, S. J., Kim, J. G., Jung, M. Y., Kim, S. J., Cha, I. T., Ghai, R., et al. (2012). Draft genome sequence of an ammonia-oxidizing archaeon, “Candidatus Nitrosopumilus sediminis” AR2, from Svalbard in the Arctic Circle. *J. Bacteriol.* 194, 6948–6949. doi: 10.1128/JB.01869-12
- Pester, M., Rattei, T., Flechl, S., Gröngroft, A., Richter, A., Overmann, J., et al. (2012). AmoA-based consensus phylogeny of ammonia-oxidizing archaea and deep sequencing of amoA genes from soils of four different geographic regions. *Environ. Microbiol.* 14, 525–539. doi: 10.1111/j.1462-2920.2011.02666.x
- Piontek, J., Galgani, L., Nöthig, E.-M., Peeken, I., and Engel, A. (2021). Organic matter composition and heterotrophic bacterial activity at declining summer sea ice in the central Arctic Ocean. *Limnol. Oceanogr.* 66, 1–20. doi: 10.1002/lno.11639
- Pruesse, E., Peplies, J., and Glöckner, F. O. (2012). SINA: Accurate high-throughput multiple sequence alignment of ribosomal RNA genes. *Bioinformatics* 28, 1823–1829. doi: 10.1093/bioinformatics/bts252
- Rapp, J. Z., Fernández-Méndez, M., Bienhold, C., and Boetius, A. (2018). Effects of Ice-Algal aggregate export on the connectivity of bacterial communities in the Central Arctic Ocean. *Front. Microbiol.* 9, 1035. doi: 10.3389/fmicb.2018.01035
- Reiswig, H. (1971a). *In situ* pumping activities of tropical Demospongiae. *Mar. Biol.* 9, 38–50. doi: 10.1007/BF00348816
- Reiswig, H. (1971b). Particle feeding in natural populations of three marine demosponges. *Biol. Bull.* 141, 568–591. doi: 10.2307/1540270
- Roberts, E. M., Mienis, F., Rapp, H. T., Hanz, U., Meyer, H. K., and Davies, A. J. (2018). Oceanographic setting and short-timescale environmental variability at an Arctic seamount sponge ground. *Deep. Res. Part I Oceanogr. Res. Pap.* 138, 98–113. doi: 10.1016/j.dsr.2018.06.007
- Roden, G. I. (1987). “Effect of seamounts and seamount chains on ocean circulation and thermohaline structure,” in *Geophysical Monograph Series: Seamounts Islands Atolls* 43, 335–354. doi: 10.1029/gm043p0335
- Roden, G. I. (1991). Mesoscale flow and thermohaline structure around Fieberling seamount. *J. Geophys. Res.* 96, 11163–11672. doi: 10.1029/91jc01747
- Rogers, A. D. (2018). “The Biology of Seamounts: 25 Years on,” in *Adv. Mar. Biol.* 79, 137–224. doi: 10.1016/bs.amb.2018.06.001
- Roussel, E. G., Sauvadet, A. L., Chaduteau, C., Fouquet, Y., Charlou, J. L., Prieur, D., et al. (2009). Archaeal communities associated with shallow to deep seafloor sediments of the New Caledonia Basin. *Environ. Microbiol.* 11, 2446–2462. doi: 10.1111/j.1462-2920.2009.01976.x
- Royer, T. C. (1978). Ocean eddies generated by seamounts in the north Pacific. *Science* 199, 1063–1064. doi: 10.1126/science.199.4333.1063-a
- Schulz, K., Janout, M., Lenn, Y. D., Ruiz-Castillo, E., Polyakov, I., Mohrholz, V., et al. (2021). On the along-slope heat loss of the boundary current in the eastern Arctic Ocean. *J. Geophys. Res. Ocean.* 126, 1–21. doi: 10.1029/2020JC016375
- Smith, J. N., Karcher, M., Casacuberta, N., Williams, W. J., Kenna, T., and Smethie, W. M. (2021). A changing arctic ocean: how measured and modeled 129I distributions indicate fundamental shifts in circulation between 1994 and 2015. *J. Geophys. Res. Ocean.* 126, 1–21. doi: 10.1029/2020JC016740
- Soetaert, K., Mohn, C., Rengstorf, A., Grehan, A., and Van Oevelen, D. (2016). Ecosystem engineering creates a direct nutritional link between 600-m deep cold-water coral mounds and surface productivity. *Sci. Rep.* 6, 1–9. doi: 10.1038/srep35057
- Soltwedel, T., Rapp, J. Z., and Hasemann, C. (2023). Impact of local iron enrichment on the small benthic biota in the deep Arctic Ocean. *Front. Mar. Sci.* 10. doi: 10.3389/fmars.2023.1118431
- Taylor, P. T., Kovacs, L. C., Vogt, P. R., and Johnson, G. L. (1979). Detailed aeromagnetic investigation of the Arctic Basin. *J. Geophys. Res.* 84, 1071–1089. doi: 10.1029/JB086iB07p06323
- Teske, A., Callaghan, A. V., and LaRowe, D. E. (2014). Biosphere frontiers of subsurface life in the sedimented hydrothermal system of Guaymas Basin. *Front. Microbiol.* 5. doi: 10.3389/fmicb.2014.00362
- Teske, A., Hinrichs, K. U., Edgcomb, V., De Vera Gomez, A., Kysela, D., Sylva, S. P., et al. (2002). Microbial diversity of hydrothermal sediments in the Guaymas Basin: Evidence for anaerobic methanotrophic communities. *Appl. Environ. Microbiol.* 68, 1994–2007. doi: 10.1128/AEM.68.4.1994-2007.2002
- Tjensvoll, I., Kutti, T., Fosså, J., and Bannister, R. (2013). Rapid respiratory responses of the deep-water sponge *Geodia barretti* exposed to suspended sediments. *Aquat. Biol.* 19, 65–73. doi: 10.3354/ab00522
- Turnewitsch, R., Dumont, M., Kiriakoulakis, K., Legg, S., Mohn, C., Peine, F., et al. (2016). Tidal influence on particulate organic carbon export fluxes around a tall seamount. *Prog. Oceanogr.* 149, 189–213. doi: 10.1016/j.pocean.2016.10.009
- Van Oevelen, D., Mueller, C. E., Lundälv, T., Van Duyl, F. C., De Goeij, J. M., and Middelburg, J. J. (2018). Niche overlap between a cold-water coral and an associated sponge for isotopically enriched particulate food sources. *PLoS One* 13, 1–16. doi: 10.1371/journal.pone.0194659
- Varliero, G., Bienhold, C., Schmid, F., Boetius, A., and Molari, M. (2019). Microbial diversity and connectivity in deep-sea sediments of the south Atlantic polar front. *Front. Microbiol.* 10. doi: 10.3389/fmicb.2019.00665

- Villinger, H., Grevenmeyer, I., Kaul, N., Hauschild, J., and Pfender, M. (2002). Hydrothermal heat flux through aged oceanic crust: Where does the heat escape? *Earth Planet. Sci. Lett.* 202, 159–170. doi: 10.1016/S0012-821X(02)00759-8
- Villinger, H. W., Pichler, T., Kaul, N., Stephan, S., Pälke, H., and Stephan, F. (2017). Formation of hydrothermal pits and the role of seamounts in the Guatemala Basin (Equatorial East Pacific) from heat flow, seismic, and core studies. *Geochemistry Geophys. Geosystems* 18, 369–383. doi: 10.1002/2016GC006665
- Visbeck, M. (2002). Deep velocity profiling using lowered acoustic Doppler current profilers: Bottom track and inverse solutions. *J. Atmos. Ocean. Technol.* 19, 794–807. doi: 10.1175/1520-0426(2002)019<0794:DVPULA>2.0.CO;2
- Vogel, S. (1977). Current induced flow through living sponges in nature. *Proc. Natl. Acad. Sci. U. S. A.* 74, 2069–2071. doi: 10.1073/pnas.74.5.2069
- von Appen, W. J., Salter, I., Nöthig, E.-M., Rabe, B., Scholz, D., Schauer, U., et al. (2017). *Physical oceanography and current meter data from mooring Karasik Accession*. (Bremerhaven, Germany: Alfred Wegener Institute, Helmholtz Centre for Polar and Marine Research). doi: 10.1594/PANGAEA.870849
- von Jackowski, A., Becker, K. W., Wietz, M., Bienhold, C., Zäncker, B., Nöthig, E.-M., et al. (2022). Variations of microbial communities and substrate regimes in the eastern Fram Strait between summer and fall. *Environ. Microbiol.* 24, 4124–4136. doi: 10.1111/1462-2920.16036
- Webster, N. S., Negri, A. P., Munro, M. M. H. G., and Battershill, C. N. (2004). Diverse microbial communities inhabit Antarctic sponges. *Environ. Microbiol.* 6, 288–300. doi: 10.1111/j.1462-2920.2004.00570.x
- Wei, M., Zhang, R., Wang, Y., Ji, H., Zheng, J., Chen, X., et al. (2013). Microbial community structure and diversity in deep-sea hydrothermal vent sediments along the Eastern Lau Spreading Centre. *Acta Oceanol. Sin.* 32, 42–51. doi: 10.1007/s13131-013-0276-6
- Wessel, P., Sandwell, D., and Kim, S.-S. (2010). The global seamount census. *Oceanography* 23, 24–33. doi: 10.5670/oceanog.2010.60
- Wickham, H. (2016). *ggplot2: elegant graphics for data analysis (Second Edition)* (New York, United States: Springer-Verlag). doi: 10.1007/978-3-319-24277-4
- Wietz, M., Bienhold, C., Metfies, K., Torres-Valdés, S., von Appen, W. J., Salter, I., et al. (2021). The polar night shift: seasonal dynamics and drivers of Arctic Ocean microbiomes revealed by autonomous sampling. *ISME Commun.* 1, 1–12. doi: 10.1038/s43705-021-00074-4
- Willenz, P., Vray, B., Maillard, M.-P., and Van de Vyver, G. (1986). A Quantitative Study of the Retention of Radioactively Labeled *E. coli* by the Freshwater Sponge *Ephydatia fluviatilis*. *Physiol. Zool.* 59, 495–504. doi: 10.1086/physzool.59.5.30156113
- Wilson, C. D., and Boehlert, G. W. (2004). Interaction of ocean currents and resident micronekton at a seamount in the central North Pacific. in *J. Mar. Syst.* 50, 39–60. doi: 10.1016/j.jmarsys.2003.09.013
- Wilson, B., Müller, O., Nordmann, E.-L., Seuthe, L., Bratbak, G., and Øvreås, L. (2017). Changes in marine prokaryote composition with season and depth over an Arctic polar year. *Front. Mar. Sci.* 4. doi: 10.3389/fmars.2017.00095
- Woodgate, R. A., Aagaard, K., Muench, R. D., Gunn, J., Björk, G., Rudels, B., et al. (2001). The Arctic Ocean boundary current along the Eurasian slope and the adjacent Lomonosov ridge: Water mass properties, transports and transformations from moored instruments. *Deep. Res. Part I Oceanogr. Res. Pap.* 48, 1757–1792. doi: 10.1016/S0967-0637(00)00091-1
- Wuchter, C., Abbas, B., Coolen, M. J. L., Herfort, L., Van Bleijswijk, J., Timmers, P., et al. (2006). Archaeal nitrification in the ocean. *Proc. Natl. Acad. Sci. U. S. A.* 103, 12317–12322. doi: 10.1073/pnas.0600756103
- Yesson, C., Clark, M. R., Taylor, M. L., and Rogers, A. D. (2011). The global distribution of seamounts based on 30 arc seconds bathymetry data. *Deep. Res. Part I Oceanogr. Res. Pap.* 58, 442–453. doi: 10.1016/j.dsr.2011.02.004
- Zhang, L., Kang, M., Xu, J., Xu, J., Shuai, Y., Zhou, X., et al. (2016). Bacterial and archaeal communities in the deep-sea sediments of inactive hydrothermal vents in the Southwest India Ridge. *Sci. Rep.* 6, 1–11. doi: 10.1038/srep25982
- Zhang, J., Kobert, K., Flouri, T., and Stamatakis, A. (2014). PEAR: A fast and accurate Illumina Paired-End read mergeR. *Bioinformatics* 30, 614–620. doi: 10.1093/bioinformatics/btt593
- Zhang, J., Sun, Q. L., Zeng, Z. G., Chen, S., and Sun, L. (2015). Microbial diversity in the deep-sea sediments of Iheya North and Iheya Ridge, Okinawa Trough. *Microbiol. Res.* 177, 43–52. doi: 10.1016/j.micres.2015.05.006
- Zhao, H., Zhang, Z., Nair, S., Zhao, J., Mou, S., Xu, K., et al. (2022). Vertically exported phytoplankton (< 20 μm) and their correlation network with bacterioplankton along a deep-sea seamount. *Front. Mar. Sci.* 9. doi: 10.3389/fmars.2022.862494